Inferring the Geometry of Convex Shapes from Their Gauss Digitization

Jacques-Olivier Lachaud[1*], David Coeurjolly[2] and Tristan Roussillon[2]

[1*]LAMA, Université Savoie Mont Blanc, CNRS, Chambéry, F-73000, France.
[2] CNRS, INSA Lyon, Université Lyon 1, Lyon, LIRIS, F-69000, France.

*Corresponding author(s). E-mail(s): jacques-olivier.lachaud@univ-smb.fr;
Contributing authors: david.coeurjolly@cnrs.fr; tristan.roussillon@liris.cnrs.fr;

Abstract

This paper studies how well we can infer the geometry of a (smooth or not) convex shape $\boldsymbol{X}$ from the convex hull $\boldsymbol{Y_h}$ of its Gauss digitization with a given gridstep $\boldsymbol{h}$. Without smoothness constraint on $\boldsymbol{X}$, we first present results concerning the proximity of facet normal vectors to the shape normal vectors, as well as a relation between the number of lattice points just above a facet and its area. Then, further results can be obtained when $\boldsymbol{X}$ is smooth, that are valid in arbitrary dimension $\boldsymbol{d}$. More precisely, we show that the boundary of $\boldsymbol{Y_h}$ is Hausdorff-close to the boundary of $\boldsymbol{X}$ with distance less than $\sqrt{\boldsymbol{d}}\boldsymbol{h}$, and that the vertices of $\boldsymbol{Y_h}$ are even much closer (some $\boldsymbol{O(h^{\frac{2d}{d+1}})}$). Our main result states that the geometric normal vectors to the facets of $\boldsymbol{Y_h}$ tend to the smooth shape normals with a speed $\boldsymbol{O(h^{\frac{1}{2}})}$, and the bound is tight. Finally we compare experimentally the performances of several normal estimators built upon the normal vectors to the facets of $\boldsymbol{Y_h}$ with state-of-the-art estimators. We also perform statistical analyses over the facets of digitized convex hulls, like their area, diameter or width as a function of the digitization gridstep. Both our new theoretical properties and our numerical experiments confirm that the convex hull of a digitized shape provide relevant information on the geometry of the underlying Euclidean convex shape, and can be used to construct fast and accurate geometric estimators.

Keywords: Geometric inference, Gauss digitization, Convex hull geometry, Digital normal estimation, Digital geometry

1 Introduction

Many works aim at inferring a shape geometry from sampled data. We study here the Gauss digitization: given a gridstep $h > 0$, the *Gauss digitization* of some $X \subset \mathbb{R}^d$ is the set of lattice points $h\mathbb{Z}^d \cap X$. Following this model, inferring a global or local geometrical property on X from its digitization boils down to the study of the convergence of some discrete estimated values, to the expected quantities defined on X, as h tends to zero. For instance, in 2D, when h is sufficiently small, the digitized boundary is shown to have the same topology as the input shape boundary when it is sufficiently smooth [1, 2]. Classical results from Huxley [3] relate the area of a smooth strictly convex shape to the number of lattice points of its digitization. Klette and Žunić [4] extend these convergence results to moments estimation. For results valid in arbitrary dimension d, we can mention that the boundary of a smooth shape and its

digitized boundary are at a Hausdorff distance no greater then $\frac{\sqrt{d}}{2}h$ [5].

For local geometry, understanding the discrete affine geometry of digitized shapes, i.e. its tangential structure, has been a widespread approach [6, 7]. Hence recognizing pieces of digital straight lines or planes is a common way to determine the local tangential geometry of digitized shapes, with however few theoretical results on geometric convergence (see related works below). Straightness is also related to convexity: it is used to define convexity [8], has very nice arithmetic and combinatorics properties [9], while its characteristics are related to the local tangent plane. Recent plane-probing algorithms [10, 11] analyze the local affine geometry of digitized boundaries using separation properties.

The common feature between all these discrete methods is that their holy grail is to recover the geometry of the convex hull when the shape is (at least locally) digitally convex, while hopefully keeping an interesting behavior in non-convex parts. The objective of this paper is precisely to determine if the convex hull of the digitization of a convex shape is an accurate local approximation of the geometry of the convex shape. This work provides bounds on the Hausdorff distance between the convex hull of the digitized set and the smooth shape boundary, tight bounds between the two normal vector fields. This work thus indicates the best results you can expect when only using linear geometry to analyze digitized convex shapes.

2 Related works

Affine geometry.

The local affine geometry of the digitized boundary is clearly related to the shape tangential characteristics. If most methods ignore the specificities of lattice data and rely on regression, smooth approximations or kernel convolutions and offer *a priori* no convergence results, several methods do take into account those specificities. We recall that an estimator has order $\beta > 0$ whenever its estimation presents an error bounded by some $O(h^\beta)$, and hence the error tends to 0 with finer sampling. In 2D, binomial derivatives achieve convergence with order $\frac{2}{3}$ [12]. Using Taylor-Lagrange inequality and a roughness criterion gives derivative estimates with order $\frac{1}{2}$ [13]. Both methods require a user given scale parameter. The maximal digital straight segment (MDSS) approach [14] is a parameter-free 2D method with a convergence order of $\frac{1}{3}$ worst case and $\frac{2}{3}$ on average. In 3D, on-surface convolutions [15] are more effective than digital straightness methods [16, 17], but with no theoretical guarantees. The only methods achieving proven normal convergence in 3D for smooth enough shapes are a discretization of Voronoi covariance measure [18] with order $\frac{1}{8}$ [19] and digital integral invariants [20] with the better order $\frac{2}{3}$ [21]: both methods require an optimal scale parameter and behave quite similarly in practice (meaning on shapes coming from real-world 3D images).

Convexity and Digital Convexity.

In 2D, classical results from Huxley [3] relate the area of a smooth strictly convex shape to the number of lattice points of its digitization. Klette and Žunić [4] extend these convergence results to moments estimation. Convergence of perimeter estimators for digitized convex shapes are reported in [22]. Convexity is also exploited in [23] to relate convex polygon edges to digital straight segments of its digitization, leading to the MDSS tangent convergence result [14]. The literature on point counting within lattice polytopes is considerable, since it is related to many enumeration and optimization problems (see, for instance, [24, 25]). Another classical topic is determining the geometric accuracy of the best possible polytope with n facets approximating a smooth convex shape [26], but this requires knowing the input shape.

Outline and contributions.

After recalling some essential notions in Section 3, Section 4 studies the general case of digitizing an arbitrary compact convex shape and of inferring its affine geometry from the convex hull of the sampled points. Lemma 2 links the facet normal vectors to the shape normal vectors. Theorem 4 relates the number of lattice points just above a facet and the facet area: if the facet area is greater than some bound, then there is at least one exterior lattice point just above this facet, and Lemma 2 holds there. Section 5 studies the case of smooth convex shapes, which happens to

be more fruitful. We can then sandwich the original shape between the digitized convex hull and its dilation by a ball of radius $\sqrt{d}h$ (Theorem 6). Vertices of the convex hull are shown asymptotically much closer to the smooth shape boundary than expected (Theorem 8). This explains *a posteriori* why the convex hull is an aestetically pleasing approximation of the underlying smooth convex shape (see Figure 3). Our main result is Theorem 9, which shows the convergence of the normal vectors to the facets of the convex hull toward the normal vectors of the input smooth convex shape, with a tight order $\frac{1}{2}$. The result is valid in arbitrary dimension and the constant is explicitly related to the reach of the shape. In Section 6, we propose several new normal vector estimators for digitized convex shapes, which exploit the normal vectors to the convex hull facets, and we compare them experimentally with several classical normal estimators of the literature. Section 7 checks the asymptotic behavior of several geometric features along digitized convex hulls (facet area, width, diameter, distance to smooth shape). Finally Section 8 concludes and gives some perspectives. This paper is an extension of the conference paper [27], where Section 6 and Section 7 constitute the additional contents.

3 Preliminaries

In the following, we only consider compact convex sets of the Euclidean space with non-empty interior. Hence compact or bounded is implicit in all statements. The topological boundary of a compact set S is denoted ∂S, its interior $\mathring{S} := S \setminus \partial S$. The d-dimensional volume of S is written $\mathrm{Vol}^d(S)$ (here taking the Lebesgue or the Hausdorff measure is equivalent in our context). The scalar product of two vectors $\mathbf{u}, \mathbf{v}$ of $\mathbb{R}^d$ is denoted by $\mathbf{u}\cdot\mathbf{v}$ and the Euclidean norm of $\mathbf{u}$ is $\|\mathbf{u}\| := \sqrt{\mathbf{u}\cdot\mathbf{u}}$. The Euclidean distance between a point $\mathbf{x}$ and the set S is $\mathrm{d}_{\mathbf{E}}(\mathbf{x}, S) := \min_{\mathbf{s}\in S} \|\mathbf{s}-\mathbf{x}\|$.

Support function, normal cone and vector. Given a convex set S, we denote by ϕ_S its *support function*, such that $\phi_S : \mathbf{w} \in \mathbb{R}^d \mapsto \max_{\mathbf{x}\in S} \mathbf{w}\cdot\mathbf{x} \in \mathbb{R}$. We recall the main property of the support function [28, §1.7.1] (see Figure 1):

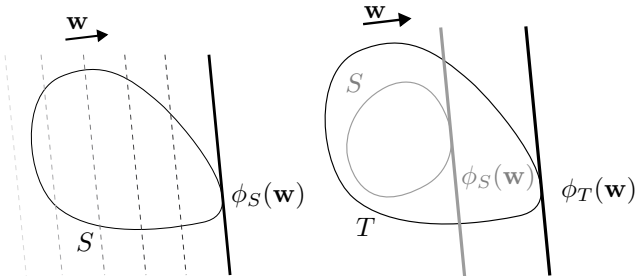

Fig. 1 Illustration of the support function definition and Theorem 1 in dimension 2.

Theorem 1. *For $S \subset T$ two convex sets of $\mathbb{R}^d$, $\forall \mathbf{w} \in \mathbb{R}^d, \phi_S(\mathbf{w}) \leqslant \phi_T(\mathbf{w})$.*

For a given unit vector $\mathbf{w} \in \mathbb{R}^d$, if the point $\mathbf{p} \in S$ satisfies $\mathbf{p}\cdot\mathbf{w} = \phi_S(\mathbf{w})$, then $\mathbf{p} \in \partial S$ and we say that $\mathbf{w}$ is a *normal vector to S at $\mathbf{p}$*. For any $\mathbf{p} \in \partial S$, the *normal cone to S at $\mathbf{p}$* is the set of normal vectors to S at $\mathbf{p}$, and is denoted by $\mathrm{N}_S(\mathbf{p})$. Note that the normal cone is reduced to one vector when ∂S is twice differentiable at $\mathbf{p}$ and we speak of *the normal vector to S at $\mathbf{p}$*.

Gauss digitization, digitized boundary, digitized convex hull. The *gridstep* is a real positive number denoted by h. The *Gauss digitization* at gridstep h of some compact $X \in \mathbb{R}^d$ is the finite set $\mathrm{D}_h(X) := h\mathbb{Z}^d \cap X$.

Let H_h be the hypercube $h[-\frac{1}{2}, \frac{1}{2}]^d$. For any *digital set* $Z \subset h\mathbb{Z}^d$, the *voxel representation of Z* is $\mathcal{Q}_h Z := Z \oplus H_h$ (and is a union of axis-aligned cubes with edge length h centered on each digital point of Z). The *(digitized) h-boundary* of a subset $S \subset \mathbb{R}^d$ is $\partial_h S := \partial \mathcal{Q}_h \mathrm{D}_h(S)$ (e.g., see [5]). Let $(\mathbf{e}_i)_{i=1,\ldots,d}$ be the canonical orthonormal basis of $\mathbb{Z}^d$. For any $z \in Z$, and if $z' := z \pm h\mathbf{e}_i$ is not in Z, we call the pair (z, z') a *surfel* of Z. Clearly, the segment $[z, z']$ crosses $\partial_h Z$ at exactly one point, which is the center of the face of $z \oplus H_h$ common with $z' \oplus H_h$.

Finally, the digital set $\mathrm{D}_h(X)$ is written X_h to shorten notations. The *digitized convex hull Y_h of X* is $Y_h := \mathrm{CvxH}(X_h)$ (where $\mathrm{CvxH}(\cdot)$ stands for the convex hull). *The objective of the paper is to show how we can infer the geometry of X from the geometry of Y_h.* We refer to Fig. 2 and 3 for 2D and 3D illustrations.

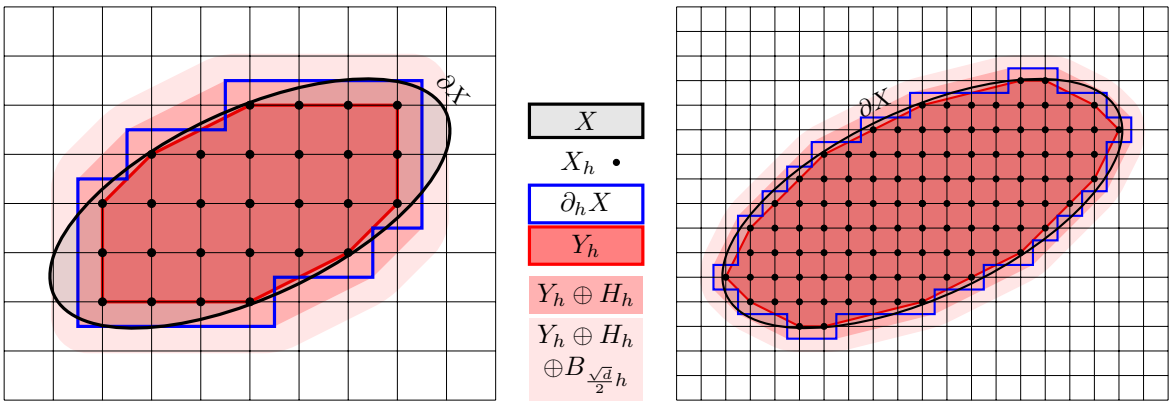

Fig. 2 2D illustration of the main notations: the convex shape X, its Gauss digitization X_h, the convex hull of the digitization Y_h and convex sets used in Theorem 6, Section 5 ($Y_h \oplus H_h$, and $Y_h \oplus H_h \oplus B_{\frac{\sqrt{d}}{2}h}$).

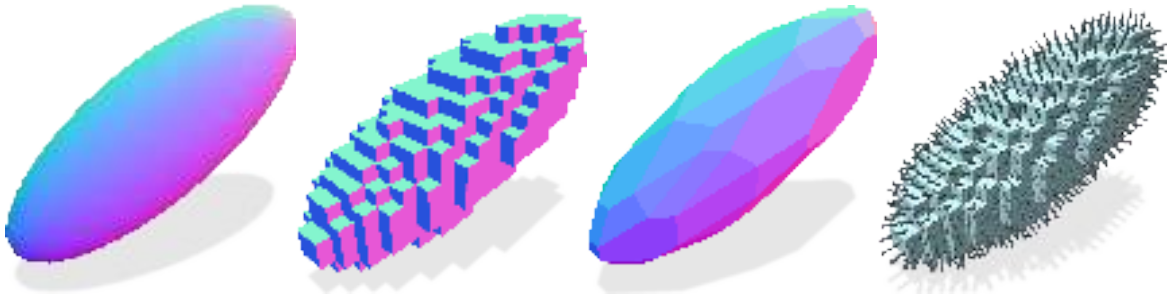

input shape X | X_h seen as voxels (i.e. $\partial_h X$) | digitized convex hull Y_h | $\partial_h X$ with facet normals

Fig. 3 3D illustration of notations and concepts, from left to right: input convex shape X, its digitization $X_h := X \cap h\mathbb{Z}^d$ seen as a collection of cubes (visually equivalent to the h-boundary $\partial_h X$), its digitized convex hull $Y_h := \mathrm{CvxH}(X_h)$, the h-boundary $\partial_h X$ with the normals of the closest facet on Y_h. The three left images are rendered with material "normal", i.e. the displayed color corresponds to the normal vector direction.

4 Properties for digitized general convex shapes

This section focuses on the geometric properties of digitized convex shape, without strong specific assumptions on the input convex shape. We will see that only partial results can be achieved in this context. For instance, accurate normal estimations are achieved around the inscribed circle center of facets (Lemma 2). Theorem 4 together with Corollary 3 allow to translate the previous result onto digitized convex hulls, in places where facets have a non negligible area. This motivates the study of input convex shapes with smoothness property in the next section, for which we will achieve much stronger approximation results.

Let X be a compact convex shape of $\mathbb{R}^d$ (smooth or not). The next lemma states that if the shape boundary ∂X is close to a facet of a (convex) polytope inscribed in X, then the normal of this facet and the normal of a nearby point $\mathbf{x}$ of ∂X are close to each other, and, the closer the points, the closer the normals. Besides, the further the projection of $\mathbf{x}$ is from the boundary of the facet, the closer are the normals (see Figure 4 for an illustration). Note that if $\mathbf{x}$ projects onto the intersection of two facets, then this Lemma does not entail any particular proximity between the facet normal and the shape normal.

Lemma 2. *Let $Y \subset X$ be a convex polytope (i.e., $Y = \mathrm{CvxH}(V)$, where V is a finite subset of X). Let $\mathbf{x}$ be an arbitrary point of ∂X, and $\mathbf{n} \in \mathrm{N}_X(\mathbf{x})$.*

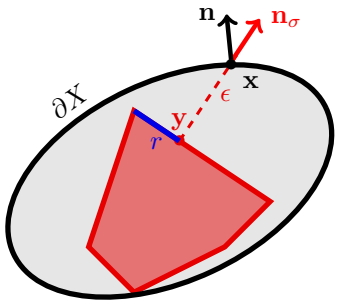

Fig. 4 Illustration of Lemma 2. Point $\mathbf{x}$ is any point on the convex shape boundary ∂X and $\mathbf{y}$ is its closest point on the polytope Y. The angle deviation between the normal to ∂Y at $\mathbf{y}$ and the normal to ∂X at $\mathbf{x}$ depends on both the distance $\epsilon := \|\mathbf{x}-\mathbf{y}\|$ and the distance r of $\mathbf{y}$ to the boundary of its containing facet σ.

Let $\mathbf{y}$ *be the closest point of* $\mathbf{x}$ *on* ∂Y *(which is unique). Assume* $\mathbf{y}$ *is contained in only one facet (say* σ*) of* Y*, with unit normal vector* $\mathbf{n}_\sigma$*. Then the normal vector* $\mathbf{n}_\sigma$ *to* Y *and the normal vector* $\mathbf{n}$ *to* X *are related as:*

$$\begin{array}{c}\mathbf{n}\cdot\mathbf{n}_\sigma \geqslant 0,\\ \sin^2\angle(\mathbf{n},\mathbf{n}_\sigma) \leqslant \frac{\epsilon^2}{\epsilon^2+r^2},\end{array} \quad \textit{with} \quad \left\{\begin{array}{l}\epsilon := \|\mathbf{x}-\mathbf{y}\|,\\ r := \mathrm{d}_{\mathbf{E}}(\mathbf{y},\partial\sigma).\end{array}\right.$$

Proof Since $\mathbf{y}\in Y\subset X$ and using the support function of X, we have immediately (see Theorem 1): $\mathbf{y}\cdot\mathbf{n}\leqslant\phi_Y(\mathbf{n})\leqslant\phi_X(\mathbf{n})=\mathbf{x}\cdot\mathbf{n}$. Since the projection onto a (compact) convex set follows the normal direction, we set $\mathbf{x}=\mathbf{y}+\epsilon\mathbf{n}_\sigma$. Substituting above gives

$$\mathbf{y}\cdot\mathbf{n}\leqslant(\mathbf{y}+\epsilon\mathbf{n}_\sigma)\cdot\mathbf{n},\ \text{therefore},\quad 0\leqslant\epsilon\mathbf{n}_\sigma\cdot\mathbf{n}.$$

Either $\epsilon>0$ and we conclude for the relation $\mathbf{n}\cdot\mathbf{n}_\sigma\geqslant 0$, or $\epsilon=0$ and $\mathbf{x}=\mathbf{y}$ which implies $\sigma\subset\partial X$ and $\mathrm{N}_X(\mathbf{x})=\mathrm{N}_Y(\mathbf{x})=\{\mathbf{n}_\sigma\}$, hence $\mathbf{n}_\sigma=\mathbf{n}$ and we also conclude.

For the second relation, let us project $\mathbf{n}$ onto the plane containing σ. This gives the vector $\mathbf{n}'=\mathbf{n}-(\mathbf{n}\cdot\mathbf{n}_\sigma)\mathbf{n}_\sigma$. If $\mathbf{n}'=\mathbf{0}$ then $\mathbf{n}=\mathbf{n}_\sigma$ and the relation is obvious. Otherwise, by the compactness of σ, the ray from point $\mathbf{y}$ in direction $\mathbf{n}'$ hits the boundary of σ at one point $\mathbf{a}$. We can write $\mathbf{a}=\mathbf{y}+s\frac{\mathbf{n}'}{\|\mathbf{n}'\|}$ with s the (positive) distance from $\mathbf{y}$ to $\mathbf{a}\in\partial\sigma$. Note that $s\geqslant r$ by hypothesis.

Since $\mathbf{a}\in\sigma\subset Y\subset X$, we have $\mathbf{a}\in X$ and using the support function of X, we get: $\mathbf{a}\cdot\mathbf{n}\leqslant\sup_{\mathbf{p}\in X}\mathbf{p}\cdot\mathbf{n}=\phi_X(\mathbf{n})=\mathbf{x}\cdot\mathbf{n}$. It implies $(\mathbf{x}-\mathbf{a})\cdot\mathbf{n}\geqslant 0$. We can decompose $\mathbf{x}-\mathbf{a}=\mathbf{x}-\mathbf{y}+\mathbf{y}-\mathbf{a}=\epsilon\mathbf{n}_\sigma-s\frac{\mathbf{n}'}{\|\mathbf{n}'\|}$. It follows that

$$-s\frac{\mathbf{n}'\cdot\mathbf{n}}{\|\mathbf{n}'\|}+\epsilon\mathbf{n}_\sigma\cdot\mathbf{n}\ =(\mathbf{x}-\mathbf{a})\cdot\mathbf{n}\geqslant 0\,,$$

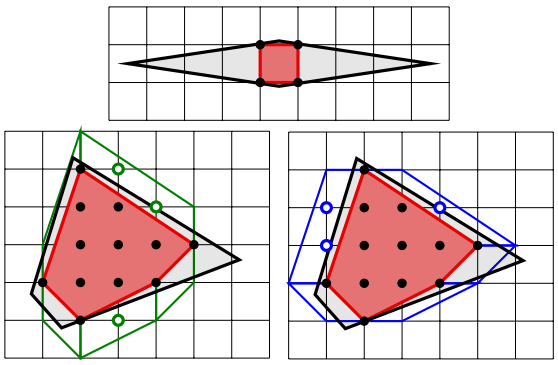

Fig. 5 Digitizations of arbitrary convex shapes: ∂X (in red) can be very far away from ∂Y_h (in black, top); however there are exterior points close to long enough edges, depending on the x- (bottom left, in green) or y-component (bottom right, in blue) of the edge vector, so ∂X is at a distance less than h near these points.

and,

$$-s\sqrt{1-(\mathbf{n}_\sigma\cdot\mathbf{n})^2}+\epsilon\mathbf{n}_\sigma\cdot\mathbf{n}\geqslant 0,$$

since simple calculations give $\mathbf{n}'\cdot\mathbf{n}=\mathbf{n}'\cdot\mathbf{n}'=1-(\mathbf{n}_\sigma\cdot\mathbf{n})^2$ (both $\mathbf{n}$ and $\mathbf{n}_\sigma$ are unit vectors). Posing $c=\mathbf{n}_\sigma\cdot\mathbf{n}$ and recalling that the first relation implies that $c\geqslant 0$, we derive

$$\epsilon c\geqslant s\sqrt{1-c^2}\,,$$

leading to

$$c^2\geqslant\frac{s^2}{s^2+\epsilon^2}$$

and

$$1-c^2\leqslant\frac{\epsilon^2}{s^2+\epsilon^2}.$$

Now $\sin\angle(\mathbf{n}_\sigma,\mathbf{n})=\frac{\|\mathbf{n}'\|}{\|\mathbf{n}\|}=\sqrt{1-c^2}$. The result follows since $r\leqslant s$. □

In the following corollary (proof is in Appendix A), we consider as convex polytope Y the convex hull Y_h of $X_h:=\mathrm{D}_h(X)$. If we define for each surfel its normal estimation as the normal vector to the closest facet on Y_h, then this corollary states a kind of multigrid convergence theorem for this normal estimator. However the convergence is influenced by the size of facets and by the relative position of surfels with respect to facet centers.

Corollary 3. *Let* $(\mathbf{z},\mathbf{z}')$ *be a surfel of* X_h*. Let* $\mathbf{y}$ *be the nearest point on* ∂Y_h *to* $\mathbf{z}'$ *and let* σ *be a facet of* Y_h *containing* $\mathbf{y}$*, with normal vector* $\mathbf{n}_\sigma$ *(see Figure 6). We have:*

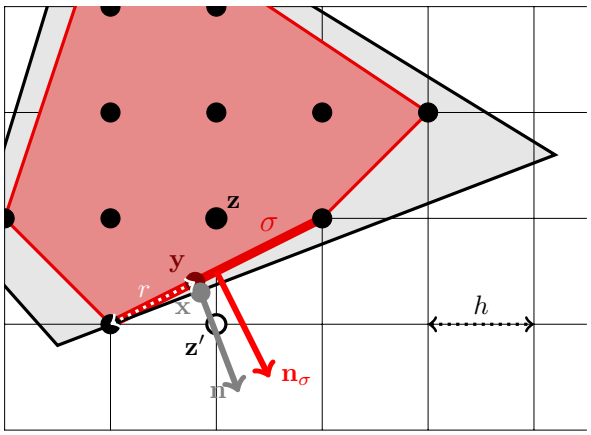

Fig. 6 Illustration of Corollary 3. We keep mostly the notations of Figure 4 for the boundary ∂X in black (inside is grey) and convex hull Y_h in red. Given a surfel $(\mathbf{z}, \mathbf{z}')$ (so $\mathbf{z} \in X_h$ as a black filled disk and $\mathbf{z}' \notin X_h$ as a black circle), the point $\mathbf{y}$ is the closest point to $\mathbf{z}'$ on ∂Y_h and it is contained in the facet σ (thicker red straight segment). If $\mathbf{x}$ is the point of ∂X lying on $[\mathbf{x}, \mathbf{z}'[$, then the normal vector $\mathbf{n}$ to ∂X at $\mathbf{x}$ is close to the facet normal vector $\mathbf{n}_\sigma$.

- *there exists* $\mathbf{x} \in \partial X \cap [\mathbf{y}, \mathbf{z}'[$, *that is at a distance less than* h *from* $\mathbf{y}$,
- *for any* $\mathbf{n} \in \mathrm{N}_X(\mathbf{x})$, $\sin^2 \angle(\mathbf{n}, \mathbf{n}_\sigma) \leqslant \frac{1}{1+(r/h)^2}$, *if* $r := \mathrm{d}_{\mathbf{E}}(\mathbf{y}, \partial\sigma)$.

The previous corollary states a convergence of normal vectors of Y_h towards normal vectors of X. It means that the point where the best estimation will be obtained is around the center of the inscribed circle/sphere of the facet. However it leaves unclear where the exterior lattice points of boundary surfels are projected onto their nearest facet: perhaps no such point exists above this center, especially if the facet is small or elongated. The following theorem shows that there are indeed exterior lattice points just above the interior of facets of Y_h, for long enough edges in 2D or wide enough triangles in 3D.

We say that a d-simplex σ of vertices $(p_1, \ldots, p_d)$ in $h\mathbb{Z}^d$ is *primitive* if $\mathrm{CvxH}\,(\sigma) \cap h\mathbb{Z}^d = \{p_1, \ldots, p_d\}$. The $d-1$-dimensional measure of the projection of σ onto a plane orthogonal to the axis $i \in \{1, \ldots, d\}$ is denoted by $A_i(\sigma)$ (informally the length or the area of the projected simplex). See Figure 5 for a 2D illustration of where lie the lattice points that are not in X but close to Y_h.

Theorem 4. *For $d \in \{2, 3\}$, let σ be a primitive edge ($d = 2$) or a primitive triangle ($d = 3$) of ∂Y_h. Then, there are (at least) k lattice points of $h\mathbb{Z}^d$ not in X at a distance strictly less than h from σ, where k follows:*

- *$d = 2$: then $k = \max_{i\in\{1,2\}}(A_i(\sigma)/h) - 1$,*
- *$d = 3$: then $k = \max_{i\in\{1,2,3\}}(A_i(\sigma)/h^2) - \frac{1}{2}$.*

Otherwise said, if a segment of ∂Y_h has one component strictly greater than h, and a triangle has one projected area strictly greater than $\frac{1}{2}h^2$, then there exists at least one close exterior lattice point not in X that projects in $\mathring{\sigma}$ along some $\pm\mathbf{e}_i$.

Proof Let us start with the case $d = 2$. Let $\sigma = (p, q)$ be a primitive edge of ∂Y_h. Let $\mathbf{t} = \pm h\mathbf{e}_i$, $i \in \{1, 2\}$ be an axis lattice vector such that $p' := p + \mathbf{t} \notin X$ and $q' := q + \mathbf{t} \notin X$. Indeed, the half plane going through (p, q) includes Y_h on one side, and the interior of the other side is empty of points of $X \cap h\mathbb{Z}^d$ (otherwise σ cannot be an edge of the convex hull). At least two vectors in $\{\pm h\mathbf{e}_i\}_{i\in\{1,2\}}$ point outside this half plane. Hence picking one of them as $\mathbf{t}$ gives $p' := p + \mathbf{t} \notin X$ and $q' := q + \mathbf{t} \notin X$. Let P be the parallelogram $\mathrm{CvxH}\,(\{p, q, p', q'\})$ and we denote by k the number of lattice points in the interior of P. Following standard notations, the number of lattice points hitting a set X of $\mathbb{R}^d$ is written $\mathcal{L}_h(X) := \#\left(\mathrm{D}_h\left(X\right)\right)$. We use Pick's theorem to bound k from below:

$$\mathrm{Vol}^2\left(\frac{1}{h}P\right) = \mathcal{L}_h(\mathring{P}) + \frac{1}{2}\mathcal{L}_h(\partial P) - 1 \quad \text{(Pick's thm)}$$
$$= k + 1. \quad \text{(since } \partial P \text{ hits 4 points exactly)}$$

These k interior points are necessarily outside X, otherwise they would be in Y_h and (p, q) would not be an edge of ∂Y_h. Noticing that $\mathrm{Vol}^2\left(\frac{1}{h}P\right) = \frac{1}{h^2}|\det(q - p, \mathbf{t})| = \frac{1}{h}|(q - p)_i| = A_i(\sigma)/h$ and using both directions $i \in \{1, 2\}$, we have found k lattice points not in X but strictly inside a parallelogram touching Y_h with width at most h. This concludes.

The case $d = 3$ is harder as there are lattice polyhedra with infinite volume that hits a few lattice points[1]. Let $\sigma = (p, q, r)$ be a primitive triangle of ∂Y_h. Let $\mathbf{t} = \pm h\mathbf{e}_i$, $i \in \{1, 2, 3\}$ be an axis lattice vector such that $p' := p + \mathbf{t} \notin X$, $q' := q + \mathbf{t} \notin X$ and $r' := r + \mathbf{t} \notin X$ (at least one exists for the reason mentioned above). Let P be the triangular prism $\mathrm{CvxH}\,(\{p, q, r, p', q', r'\})$ and we denote by k the number of lattice points in the interior of P. We exploit

[1] The tetrahedron $\{(0, 0, 0), (1, 0, 0), (0, 1, 0), (1, 1, j)\}$, for instance, hits exactly 4 lattice points whatever the value $j \in \mathbb{Z}$.

here Reeve's result [29, Theorem I], valid for any integer $n \geqslant 1$ and full-dimensional lattice convex polytope P:

$$2(n^3-n)\mathrm{Vol}^3\left(\frac{1}{h}P\right) = 2\left(\mathcal{L}_{\frac{h}{n}}(P) - n\mathcal{L}_h(P)\right) - \left(\mathcal{L}_{\frac{h}{n}}(\partial P) - n\mathcal{L}_h(\partial P)\right) \quad (1)$$

Note that we have $\mathcal{L}_{\frac{h}{n}}(P) = \mathcal{L}_h(nP)$ (where nP stands for homothety of P centered at the origin by the factor n). We use the relations above with the dilation factor $n = 2$.

$\mathcal{L}_h(P) = 6 + k$ and $\mathcal{L}_h(\partial P) = 6$ are obvious from the fact that the triangular face is primitive and k is the number of interior lattice points. Dilating by two the lattice prism creates 4 similar triangles at the base, with exactly 6 lattice points on its boundary since the triangle is primitive. Then, the vector $\mathbf{t}$ being a trivial axis vector, the dilated prism is composed of 3 layers of these 4 triangles, hence 18 lattice points in total and we have $\mathcal{L}_{\frac{h}{2}}(\partial P) = \mathcal{L}_h(\partial 2P) = 18$.

Finally the prism P is assumed to contain k lattice points in its interior. The prism $2P$ is the disjoint union of 8 copies of P (translated or rotated) with disjoint interiors. So the interior of $2P$ contains $8k$ lattice points. It follows that $\mathcal{L}_{\frac{h}{2}}(P) = \mathcal{L}_h(2P) \leqslant 18 + 8k$. Inserting these values into (1) leads to:

$$\begin{aligned} 12\mathrm{Vol}^3\left(\frac{1}{h}P\right) &= 2\left(18 + 8k - 2(6+k)\right) - (18-12) \\ &= 6 + 12k. \end{aligned}$$

A short computation gives $k = \mathrm{Vol}^3\left(\frac{1}{h}P\right) - \frac{1}{2}$.

We notice again that $\mathrm{Vol}^3\left(\frac{1}{h}P\right) = \frac{1}{2h^3}|\det(q-p, r-p, \mathbf{t})| = \frac{1}{h^2}A_i(\sigma)$ to conclude the argument. □

The results in this section show that there are points on Y_h where the normal vector of the underlying shape can be well estimated. Furthermore, we know that the best estimations are obtained for points above large enough facets and near their inscribed sphere center. However we have no control on the radius of the inscribed sphere. Furthermore, Figure 5 shows that there are points of ∂X that can be very far away from ∂Y_h. All these elements indicate that we must require more constraints on the input shape in order to get better geometric estimates. By assuming smoothness on the shape boundary, the next section will show that we can get better estimates for X from its digitization Y_h, both in position and normal vector field estimation.

5 Properties for digitized smooth convex shapes

If we assume smoothness of the convex shape X, we can use the previous result to show the convergence of normal vectors in 2D around most edges of Y_h.

Theorem 5. *For a small enough gridstep h, if X is a convex shape of $\mathbb{R}^2$ with C^3-smooth boundary and positive curvature, then any edge σ of ∂Y_h having at least the average length of edges of ∂Y_h has a normal $\mathbf{n}_\sigma$ close to the normal $\mathbf{n}$ of the closest point of ∂X to the edge center, and more precisely $\angle(\mathbf{n}, \mathbf{n}_\sigma) \leqslant ch^{\frac{1}{3}}$, for some positive constant c.*

Proof [30, Theorem 2] tells that the number of vertices $N(Y_h)$ of ∂Y_h is some $\Theta(h^{-\frac{2}{3}})$. So the average length $L(Y_h)$ of the edges of Y_h is the perimeter of ∂Y_h divided by $N(Y_h)$. It is well known that the perimeter of Y_h approximates the perimeter of X to an order $O(h)$: one way to see it is to use Theorem 6 together with the result that, for $A \subset B$ compact convex shapes, the perimeter of A is no greater than the perimeter of B. So $L(Y_h) = \Theta(h^{\frac{2}{3}})$. According to Theorem 4 in the case $d = 2$, there are almost as many exterior lattice points as the discrete length of the nearby edge. Except for a constant number of edges (maximum 8, the ones having directions $(1,0)$ and $(1,1)$ and their 4 rotations), all the other edges have an exterior lattice point close to the center of the edge: Indeed, according to Theorem 4, the number of exterior lattice points near the edge is the greatest component of the edge vector minus 1. So there is an exterior lattice point at distance h from the edge center. For an edge σ with approximately the average length $L(Y_h)$, the estimation error between n_σ and the closest point on ∂X is (Corollary 3): $\sin^2\angle(\mathbf{n}, \mathbf{n}_\sigma) \leqslant \frac{1}{1+(L(Y_h)/2h)^2}$, the right term being equal to $\frac{1}{1+\Theta(h^{-2/3})} = \Theta(h^{\frac{2}{3}})$. Therefore, we have $\sin^2\angle(\mathbf{n}, \mathbf{n}_\sigma) = O(h^{\frac{2}{3}})$, which implies $\sin\angle(\mathbf{n}, \mathbf{n}_\sigma) = O(h^{\frac{1}{3}})$ and by Taylor expansion, $\angle(\mathbf{n}, \mathbf{n}_\sigma) = O(h^{\frac{1}{3}})$. □

Unfortunately, this result cannot be easily extended to higher dimensions, since there exist small or elongated facets starting from 3D. In fact, by using a completely different approach, we achieve below a much stronger result on normal convergence.

Before that, let us try to better understand how the geometry of Y_h and the geometry of X exhibit more relations in the case where X has a smooth boundary. The *reach* of $S \subset \mathbb{R}^d$, denoted $\text{reach}(S)$, is the infimum of the distance of the set S to its medial axis [31] (the medial axis gathers points that have at least two nearest neighbors on S). From now on, we change the smoothness condition on X and we assume that $\text{reach}(\partial X)$ is greater than some $\rho > 0$. In our context, it means that ∂X has its principal curvatures between 0 (included) and $1/\rho$ (excluded).

We start by sandwiching X between Y_h and $Y_h \oplus H_h \oplus B_{\frac{\sqrt{d}}{2}h}$, where B_r is the ball centered on $\mathbf{0}$ and of radius r. Note that it is not true in general that $X \subset Y_h \oplus H_h$, as illustrated by Figure 2.

Theorem 6. *Assume $X \subset \mathbb{R}^d$, compact, convex with $\text{reach}(\partial X) > \rho$. For all gridsteps h, $0 < h < \frac{2\rho}{\sqrt{d}}$, we have $Y_h \subset X \subset Y_h \oplus H_h \oplus B_{\frac{\sqrt{d}}{2}h}$. It follows that the convex boundary ∂X lies in the strip $Y_h \oplus H_h \oplus B_{\frac{\sqrt{d}}{2}h} \setminus \text{Int}(Y_h)$. Furthermore $\mathrm{d}_H(X, Y_h) = \mathrm{d}_H(\partial Y_h, \partial X) \leqslant \sqrt{d}h$.*

Proof We have $X_h \subset X$ so $Y_h = \text{CvxH}(X_h) \subset \text{CvxH}(X) = X$ and the first inclusion follows. By definition, the h-boundary $\partial_h X$ of X is the topological boundary of $X_h \oplus H_h$, i.e. $\partial_h X = \partial(X_h \oplus H_h)$. It implies

$$\begin{aligned}\text{CvxH}(\partial_h X) &= \text{CvxH}(\partial(X_h \oplus H_h)) \\ &= \text{CvxH}(X_h \oplus H_h) = Y_h \oplus H_h, \end{aligned} \quad (2)$$

using the commutativity of $\oplus$ and $\text{CvxH}(\cdot)$. According to [5, Theorem 1], $\mathrm{d}_H(\partial_h X, \partial X) \leqslant \frac{\sqrt{d}}{2}h$ for $h < \frac{2\rho}{\sqrt{d}}$. Hence

$$\partial X \subset \partial_h X \oplus B_{\frac{\sqrt{d}}{2}h} \quad (3)$$

and

$$\begin{aligned}\text{CvxH}(\partial X) &\subset \text{CvxH}\left(\partial_h X \oplus B_{\frac{\sqrt{d}}{2}h}\right) \quad \text{(using (3))} \\ &= \text{CvxH}(\partial_h X) \oplus B_{\frac{\sqrt{d}}{2}h}.\end{aligned}$$

Finally, we get

$$\text{CvxH}(\partial X) \subset Y_h \oplus H_h \oplus B_{\frac{\sqrt{d}}{2}h}. \quad \text{(using (2))}$$

It remains to establish the Hausdorff distance between ∂X and ∂Y_h. Since Y_h, X and $Y_h \oplus H_h \oplus B_{\frac{\sqrt{d}}{2}h}$ are all convex, we have these relations for their support functions, for any $\mathbf{w} \in \mathbb{R}^d$:

$$\phi_{Y_h}(\mathbf{w}) \leqslant \phi_X(\mathbf{w}) \leqslant \phi_{Y_h \oplus H_h \oplus B_{\frac{\sqrt{d}}{2}h}}(\mathbf{w}). \quad (4)$$

A classical result is that $\phi_{A\oplus B} = \phi_A + \phi_B$ for compact convex sets A, B [28, Theorem 1.7.5a], so it holds:

$$\phi_{Y_h \oplus H_h \oplus B_{\frac{\sqrt{d}}{2}h}}(\mathbf{w}) = \phi_{Y_h}(\mathbf{w}) + \phi_{H_h}(\mathbf{w}) + \phi_{B_{\frac{\sqrt{d}}{2}h}}(\mathbf{w}).$$

Inserting this equality in (4), and subtracting $\phi_{Y_h}(\mathbf{w})$ to the three terms give:

$$0 \leqslant \phi_X(\mathbf{w}) - \phi_{Y_h}(\mathbf{w}) \leqslant \phi_{H_h}(\mathbf{w}) + \phi_{B_{\frac{\sqrt{d}}{2}h}}(\mathbf{w}).$$

Assuming now that $\mathbf{w}$ is a unit vector, we get

$$0 \leqslant \phi_X(\mathbf{w}) - \phi_{Y_h}(\mathbf{w}) \leqslant \frac{\sqrt{d}}{2}h + \frac{\sqrt{d}}{2}h.$$

It follows that $\sup_{\mathbf{w}\in S} \|\phi_X(\mathbf{w}) - \phi_{Y_h}(\mathbf{w})\| \leqslant \sqrt{d}h$ for S the unit sphere of $\mathbb{R}^d$, which implies $\mathrm{d}_H(X, Y_h) \leqslant \sqrt{d}h$.

We finally use [32, Theorem 20], which states that "If A and B are non-empty, closed, bounded convex sets, $\mathrm{d}_H(A, B) = \mathrm{d}_H(\partial A, \partial B)$", to conclude that $\mathrm{d}_H(\partial X, \partial Y_h) \leqslant \sqrt{d}h$. □

Corollary 7. *For all gridsteps h, $0 < h < \frac{2\rho}{\sqrt{d}}$, for $\mathbf{y} \in \partial Y_h$ and any normal vector $\mathbf{w} \in \mathrm{N}_{Y_h}(\mathbf{y})$, define P as the plane orthogonal to $\mathbf{w}$ and containing $\mathbf{y}$. Then for any point $\mathbf{y}' \in P$, we have that $\mathbf{y}' + t\mathbf{w}$ is outside X for $t > \sqrt{d}h$.*

Proof Proof is in appendix. □

We now show that vertices of ∂Y_h are much closer to ∂X than the upper bound on $\mathrm{d}_H(\partial X, \partial Y_h)$ suggests, *ie.* some $\Theta(h^{\frac{3}{2}})$ instead of $\sqrt{3}h$ in 3D. This result is not really new. Most of the proof relies on the so called *Macbeath region* of a point $\mathbf{x} \in X$, that is $M_X(\mathbf{x}) := X \cap (2\mathbf{x} - X)$ (intersection of X with its central symmetry around $\mathbf{x}$). Macbeath [33] introduced them to count lattice points in-between two convex bodies. Similar arguments can be found in the proof of the upper bound of [30, Theorem II], or from [34, Theorem 4.3 and discussion]. Our proof below has the advantage of making explicit the constant in the upper-bound with respect to the reach.

Theorem 8. *Assume the convex set $X \subset \mathbb{R}^d$ has $\text{reach}(\partial X) > \rho$. Let $\mathbf{y}$ be a vertex of Y_h. It holds that, for gridsteps h, $0 < h \leqslant \rho$, $\mathrm{d}_{\mathbf{E}}(\mathbf{y}, \partial X) < \alpha_d \rho^{-\frac{d-1}{d+1}} h^{\frac{2d}{d+1}}$, where the constant α_d depends on the dimension. If h is sufficiently small, we have $\alpha_2 \approx \left(\frac{3}{2\sqrt{2}}\right)^{\frac{2}{3}}$ and $\alpha_3 \approx \frac{2}{\sqrt{\pi}}$.*

Proof Any vertex $\mathbf{y}$ of Y_h is at a distance less than h from ∂X (one of $\mathbf{y} \pm h\mathbf{e}_i, i \in \{1,\dots,d\}$, must be outside X). So $\mathrm{d}_{\mathbf{E}}(\mathbf{y},\partial X) \leqslant h$ and $\mathbf{y}$ is within the reach of ∂X by hypothesis. Let $\mathbf{x}$ be the projection on ∂X of $\mathbf{y}$ and $\mathbf{n} := \frac{\mathbf{x}-\mathbf{y}}{\|\mathbf{x}-\mathbf{y}\|}$ the unit outward normal to X at $\mathbf{x}$. The open ball B of center $\mathbf{x}-\rho\mathbf{n}$ and radius ρ is contained in X. Furthermore, $\mathbf{y}$ belongs to the straight segment $[\mathbf{x}-\rho\mathbf{n},\mathbf{x}]$.

Let $S_X := M_X(\mathbf{y}) = X \cap (2\mathbf{y}-X)$ and $S_B := M_B(\mathbf{y}) = B \cap (2\mathbf{y}-B)$ (see Figure 7). Since $B \subset X$ we have $S_B \subset S_X$, hence $\mathrm{Vol}^d(S_B) \leqslant \mathrm{Vol}^d(S_X)$. We explicit $\mathrm{Vol}^d(S_B)$ as a function of $\delta := \|\mathbf{x}-\mathbf{y}\| = \mathrm{d}_{\mathbf{E}}(\mathbf{y},\partial X)$.

It is clear that S_B is the union of two caps of a d-ball of radius ρ. Each slice of each cap is itself a $d-1$-ball of radius s, denoted by $B^{d-1}(s)$, where s depends on the distance t to $\mathbf{x}$. It is also known that $\mathrm{Vol}^{d-1}\left(B^{d-1}\right)(s) = \frac{\pi^{(d-1)/2}}{\Gamma((d+1)/2)} s^{d-1}$. Furthermore Pythagoras theorem indicates $\rho^2 = (\rho-t)^2 + s^2$, so $s = \sqrt{2\rho t - t^2}$. We compute:

$$\begin{aligned}\mathrm{Vol}^d(S_B) &= 2\int_0^\delta \mathrm{Vol}^{d-1}\left(B^{d-1}(\sqrt{2\rho t - t^2})\right) dt \\ &= 2\int_0^\delta \frac{\pi^{\frac{d-1}{2}}}{\Gamma\left(\frac{d+1}{2}\right)} \left(\sqrt{2\rho t - t^2}\right)^{d-1} dt.\end{aligned}$$

Standard integral computations gives:

- for $d = 2$, we have $\Gamma(\frac{3}{2}) = \frac{1}{2}\sqrt{\pi}$, and $\mathrm{Vol}^2(S_B) = \frac{8\sqrt{2\rho}}{3}\delta^{\frac{3}{2}} + O\left(\frac{\delta^{\frac{5}{2}}}{\sqrt{\rho}}\right)$,
- for $d = 3$, $\Gamma(2) = 1$, and $\mathrm{Vol}^3(S_B) = 2\pi\rho\delta^2 - \frac{2}{3}\pi\delta^3$,
- for $d = 4$, $\Gamma(\frac{5}{2}) = \frac{3}{4}\sqrt{\pi}$, and $\mathrm{Vol}^4(S_B) = \frac{32\pi\sqrt{2}\rho^{\frac{3}{2}}}{15}\delta^{\frac{5}{2}} + O\left(\delta^{\frac{7}{2}}\sqrt{\rho}\right)$.

For a generic bound in d, it is enough in our context —and simpler— to compute the volume of the bi-cone within S_B, hence:

$$\begin{aligned}\mathrm{Vol}^d(S_B) &\geqslant 2\int_0^\delta \mathrm{Vol}^{d-1}\left(B^{d-1}(\tfrac{t}{\delta}\sqrt{2\rho\delta - \delta^2})\right) dt \\ &= 2\int_0^\delta \frac{\pi^{\frac{d-1}{2}}}{\Gamma\left(\frac{d+1}{2}\right)} \left(\frac{t}{\delta}\sqrt{2\rho\delta - \delta^2}\right)^{d-1} dt \\ &= \Theta\left(\rho^{\frac{d-1}{2}}\delta^{\frac{d+1}{2}}\right).\end{aligned}$$

We may now use Minkowski's theorem [35] on S_X. The volume of S_X cannot exceed $(2h)^d$. Indeed, if this is the case, then S_X must contain at least two other lattice points $\mathbf{z}$ and $\mathbf{z}'$ symmetric around $\mathbf{y}$ ($\mathbf{y}-\mathbf{z} = \mathbf{z}'-\mathbf{y}$) (Figure 7). But both $\mathbf{z},\mathbf{z}' \in X$, so $\mathbf{z}$ and $\mathbf{z}'$ belong to X_h and thus Y_h. Yet $\mathbf{y}$ is a vertex of the convex polytope Y_h and cannot be in the middle of two other points of Y_h. It follows that

$$(2h)^d > \mathrm{Vol}^d(S_X) \geqslant \mathrm{Vol}^d(S_B) \geqslant \Theta\left(\rho^{\frac{d-1}{2}}\delta^{\frac{d+1}{2}}\right).$$

We achieve this upper bound for vertex distance $\delta < \alpha_d h^{\frac{2d}{d+1}}/\rho^{\frac{d-1}{d+1}}$. Constants α_2 and α_3 are derived from the more precise formula above. □

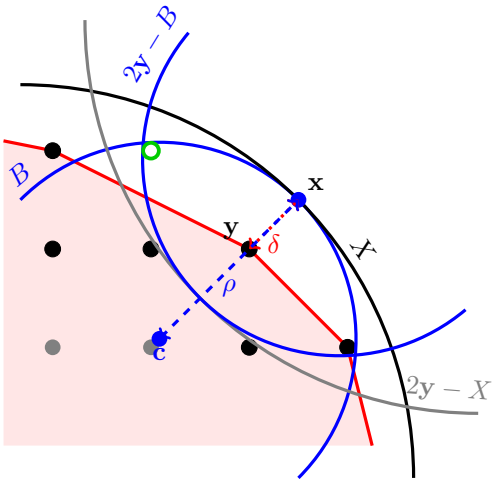

Fig. 7 Illustration for the proof of Theorem 8.

One can check in practice that these theoretical bounds are indeed reached in 2D and 3D, on digitizations of ellipses for instance, and that the constants are quite tight (see Figure 18, page 17).

Theorem 9 below is our main result: it shows that the normal vectors to the facets of the digitized convex hull converge towards the normal vectors of the smooth convex shape, for small enough gridstep h, and that the speed of convergence is proportional to $\sqrt{h/\rho}$.

Theorem 9. *Assume the convex set $X \subset \mathbb{R}^d$ has $\mathrm{reach}(\partial X) > \rho$. Let $\mathbf{y}$ be any point on the boundary ∂Y_h. The point $\mathbf{x} := \pi_{\partial X}(\mathbf{y})$ is its closest point on ∂X, and it is well known that the outer normal $\mathbf{n}$ to X at $\mathbf{x}$ is aligned with $\mathbf{x}-\mathbf{y}$. Let $\mathbf{w} \in \mathrm{N}_{Y_h}(\mathbf{y})$ be any normal vector to Y_h at $\mathbf{y}$. Let $\delta := \|\mathbf{x}-\mathbf{y}\|$. Then for gridsteps h, $0 < h < \frac{\rho}{\sqrt{d}}$, it holds that $0 \leqslant \delta < \sqrt{d}h$ and:*

$$\mathbf{n}\cdot\mathbf{w} \geqslant \frac{1-\sqrt{d}\frac{h}{\rho}}{1-\frac{\delta}{\rho}} \geqslant 1 - \sqrt{d}\frac{h}{\rho} > 0$$

$$\textit{i.e.} \quad \angle(\mathbf{n},\mathbf{w}) \leqslant O\left(\sqrt{h/\rho}\right).$$

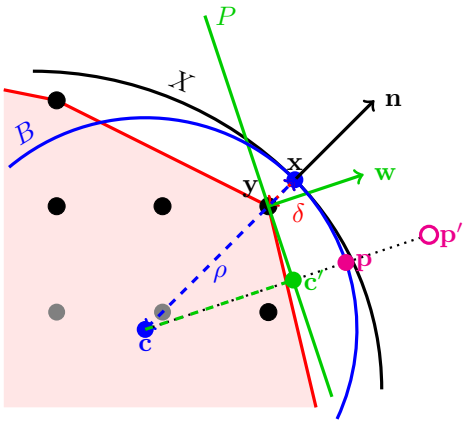

Fig. 8 Illustration for the proof of Theorem 9.

Proof See Figure 8 for an illustration. Let B be the ball centered on $\mathbf{c} := \mathbf{x} - \rho\mathbf{n}$ and of radius ρ. Since ∂X has positive reach ρ, B lies inside X. Let P be the plane containing $\mathbf{y}$ and orthogonal to $\mathbf{w}$ and let $\mathbf{c}' := \pi_P(\mathbf{c}) = \mathbf{c} - ((\mathbf{c}-\mathbf{y})\cdot\mathbf{w})\mathbf{w}$, *i.e.* the projection of $\mathbf{c}$ onto P. Letting $\delta := \|\mathbf{x}-\mathbf{y}\|$, we have $\|\mathbf{c}-\mathbf{y}\| = \rho-\delta$ since $\mathbf{c},\mathbf{y},\mathbf{x}$ are aligned.

$$\begin{aligned}(\mathbf{c}'-\mathbf{c})\cdot\mathbf{w} &= (\mathbf{c} - ((\mathbf{c}-\mathbf{y})\cdot\mathbf{w})\mathbf{w} - \mathbf{c})\cdot\mathbf{w} \\ &= (\mathbf{y}-\mathbf{c})\cdot\mathbf{w} = (\rho-\delta)\mathbf{n}\cdot\mathbf{w}. \qquad (5)\end{aligned}$$

On one side, we know that $\mathbf{p} := \mathbf{c} + \rho\mathbf{w}$ belongs to B hence also to X. On the other side, Corollary 7 entails that $\mathbf{p}' := \mathbf{c}' + \sqrt{d}h\mathbf{w}$ does not belong to X and, more precisely, that $\phi_X(\mathbf{w}) < \mathbf{p}'\cdot\mathbf{w}$. We have

$$\begin{aligned}\mathbf{p}\cdot\mathbf{w} = (\mathbf{c}+\rho\mathbf{w})\cdot\mathbf{w} &\leqslant \phi_X(\mathbf{w}) \\ &< \mathbf{p}'\cdot\mathbf{w} = (\mathbf{c}'+\sqrt{d}h\mathbf{w})\cdot\mathbf{w}.\end{aligned}$$

Using $\mathbf{w}\cdot\mathbf{w} = 1$ and (5), it follows:

$$\rho - \sqrt{d}h < (\mathbf{c}'-\mathbf{c})\cdot\mathbf{w} = (\rho-\delta)\mathbf{n}\cdot\mathbf{w}. \qquad (6)$$

Corollary 7 also implies that $\delta < \sqrt{d}h$ (otherwise $\mathbf{x}$ would be outside X). Since $h < \rho/\sqrt{d}$ by hypothesis, we have $\delta < \rho$ and $\sqrt{d}h < \rho$, so the left-hand side of (6) is positive, and so is its right hand. This entails $\mathbf{n}\cdot\mathbf{w} > 0$. Moreover

$$\mathbf{n}\cdot\mathbf{w} > \frac{\rho-\sqrt{d}h}{\rho-\delta} = \frac{1-\sqrt{d}h/\rho}{1-\delta/\rho} \geqslant 1 - \sqrt{d}\frac{h}{\rho}. \qquad (7)$$

Let $\alpha := \angle(\mathbf{n},\mathbf{w})$. So $\cos\alpha > 1-\sqrt{d}\frac{h}{\rho}$. From the above expression, it can be seen that α tends to zero as h tends to zero. Taylor expansion of $\arccos(1-\sqrt{d}\frac{h}{\rho})$ around $h = 0$ gives $\alpha < \sqrt{\frac{2\sqrt{d}}{\rho}}h + O(h^{\frac{3}{2}})$, which concludes. □

The result is tight in convergence order, and we can exhibit a simple example where the constant is almost reached (gap is less than $2^{1/4} \approx 20\%$): just consider a disk X of radius $\rho = h(k+1-\epsilon)$, k a positive integer, ϵ an arbitrary small positive real number. The convex hull Y_h has a vertical edge symmetric about the x-axis going through the lattice point $(hk, 0)$. Due to Pythagoras theorem, its two vertices are close to $\pm(hk, h\sqrt{2k})$ (up to negligible terms). Let $\mathbf{x}$ be the closest point on ∂X to the upper vertex, its normal is $\mathbf{n} \approx \frac{(k,\sqrt{2k})}{\sqrt{k^2+2k}}$. The normal to edge is $\mathbf{w} = (1,0)$. We get $\mathbf{n}\cdot\mathbf{w} = \frac{1}{\sqrt{1+2/k}}$, thus $\angle(\mathbf{n},\mathbf{w}) \approx \sqrt{\frac{2}{k}} \approx \sqrt{\frac{2h}{\rho}}$, to compare with $\sqrt{\frac{2\sqrt{2}h}{\rho}}$ of Theorem 9.

6 Normal estimation on digitized convex shapes

Theorem 9 (and to a lesser extent Corollary 3 and Theorem 5) indicates that the normal vector to facets of the digitized convex hull could be used as a discrete normal estimator on digitized convex shapes. It is quite natural to interpolate normal estimations between facets in order to smooth the result. We can also test if using a smoothing convolution kernel can enhance the result. We therefore numerically test these methods for normal estimations on digitized convex shapes, and we compare them to classical methods for normal estimation.

Figures 9, 10 and 11 illustrate qualitatively the normal estimations on two different 3D shapes: `ellipsoid` with equation $3x^2 + 2y^2 + z^2 = 90$, and `slanted ellipsoid` of equation $3x^2 + 5y^2 + 7z^2 + 5xy - 4xz = 100$. As one can observe, estimations converge toward ground truth for all estimators, while interpolation and convolution improve results.

More precisely, we compare numerically the accuracy of the following normal estimators at a surfel $(\mathbf{z},\mathbf{z}')$ of $\partial_h X$, with $\dot{\mathbf{z}} = (\mathbf{z}+\mathbf{z}')/2$ and σ the closest facet of Y_h to $\dot{\mathbf{z}}$:

CVXH The normal vector at $\dot{\mathbf{z}}$ is estimated with $\mathbf{n}_\sigma$, the normal vector to the facet σ on Y_h. If there are several facets closest to $\dot{\mathbf{z}}$, we take the average of their normal vectors.

I-CVXH The normal vector at $\dot{\mathbf{z}}$ is estimated through linear interpolation of CVXH estimator: first an estimated normal vector $\mathbf{n}_i$ at each vertex $\mathbf{v}_i$ of Y_h is defined as the linear combination of

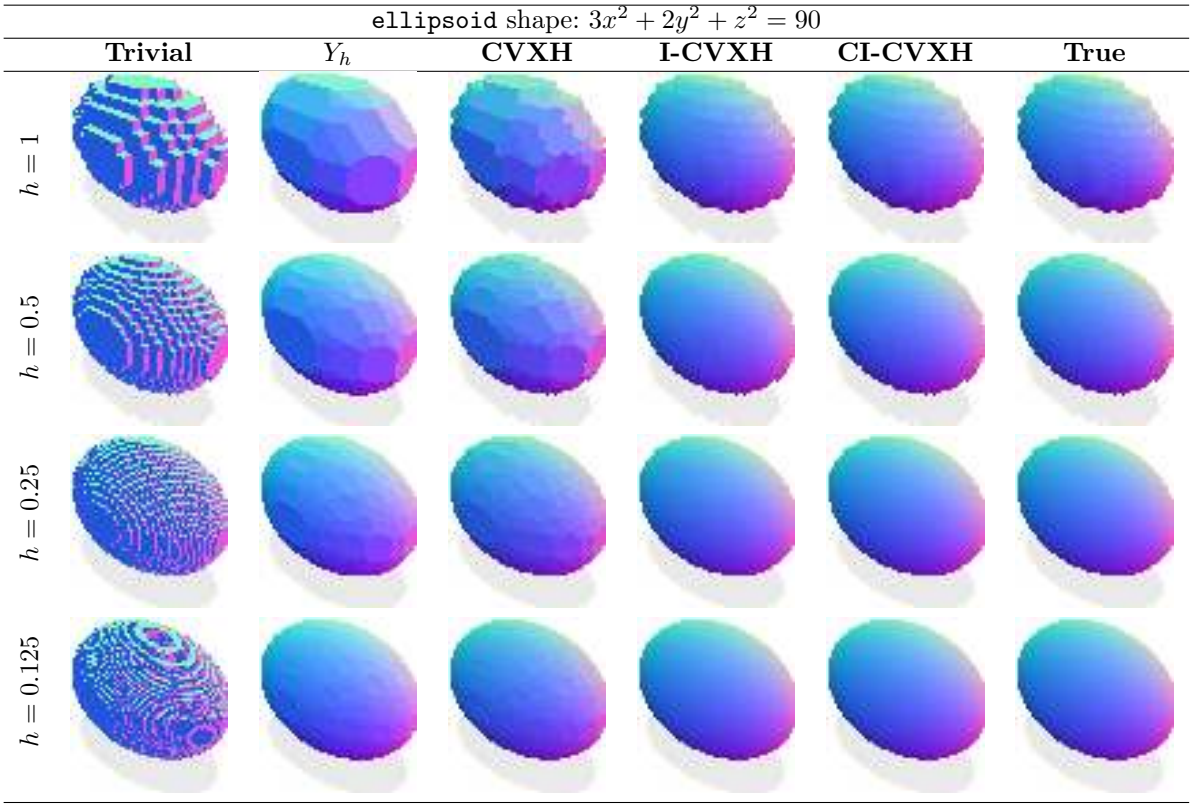

Fig. 9 Qualitative illustration of normal estimations for estimators specialized to digitized convex shapes (CVXH, I-CVXH, CI-CVXH), for finer and finer digitization of shape `ellipsoid`. Normal vectors are displayed with the normal map colormap.

the normal vector to each facet incident to $\mathbf{v}_i$, weighted by the inverse distance of $\mathbf{v}_i$ to the facet centroid. Secondly the normal vector at $\dot{\mathbf{z}}$ is then the linear combination of the normal vectors $(\mathbf{n}_j)$ of the vertices $(\mathbf{v}_j)$ of the facet σ, weighted by the inverse distance of $\pi_\sigma(\dot{\mathbf{z}})$ to each vertex $\mathbf{v}_j$.

II The digital Integral Invariant normal estimator [20, 36] is the (reoriented) smallest eigenvector of the covariance matrix of $B_r(\dot{\mathbf{z}}) \cap \mathrm{D}_h(X)$: for $r = \Theta(h^{\frac{1}{3}})$ it is proven convergent in [21] with ℓ_∞-error in $\Theta(h^{\frac{2}{3}})$.

VCM The digital Voronoi Covariance Measure [18] is the (reoriented) highest eigenvector of the covariance matrix of the projection vectors of $B_R(\dot{\mathbf{z}}) \cap \mathbb{Z}^d$ onto $\partial_h X$, restricted to projections within $B_r(\dot{\mathbf{z}})$: for $R = \Theta(h^{\frac{1}{4}})$ and $r = \Theta(h^{\frac{1}{4}})$ it is proven convergent in [19] with ℓ_∞-error in $\Theta(h^{\frac{1}{8}})$.

COV The covariance estimator estimates for any point $\dot{\mathbf{z}}$ the best planar fit to the surfel centroids of $\partial_h X$ in the ball of radius r centered on $\dot{\mathbf{z}}$. It builds the covariance matrix of these points as a 3D data set, and extracts the eigenvector corresponding to the lowest eigenvalue. Although it has been widely used in data science, we mention here the work of Mitra and Nguyen [37], which has provided theoretical bounds for such normal estimates in case of point cloud data. For an optimal radius of $r = \Theta(h^{\frac{2}{3}})$, the angle error is lower than $\Theta(h^{\frac{2}{3}})$ with high probablity.

C-Trivial The estimated normal is the convolution by the kernel $\chi_r(\mathbf{x}) := e^{-\frac{1}{1+\|\mathbf{x}\|^2/r^2}}$ of the trivial normal vectors to the surfels within the ball of radius r centered on $\dot{\mathbf{z}}$, for $r = \Theta(h^{\frac{1}{2}})$. This method is a variant of [38], but with a weighted kernel of radius adapted to the gridstep. It is also akin to the diffusion method of [15]. No theoretical convergence result is proven in the literature.

CI-CVXH The estimated normal is the convolution by the same kernel $\chi_r(\mathbf{x})$ of the I-CVXH normal vectors to surfels within the ball of radius r centered on $\dot{\mathbf{z}}$, for $r = \Theta(h^{\frac{1}{2}})$.

All experiments have been conducted on MacBook Pro, Apple M2 Max chip with 64 Gb of RAM (LPDDR5) using only sequential implementations of estimators from the `DGtal` library [39].

In Figure 12 we further compare the estimators using quantitative measures (normal angle errors in degrees). Both root mean square errors (L_2-error) and maximum error (L_∞-error) are displayed. We also display on Figure 13 the timings for each estimator on these two shapes, under several forms: as a function of the gridstep and as a function of the number of surfels. Finally, Figure 14 shows for each estimator the normal angle errors as a function of the computation time, which is indicative of a good trade-off between accuracy and computational cost.

Multigrid convergence is observed for all estimators, in L_2 or L_∞ error norm. **II** works for arbitrary (not necessarily convex) digitized boundary and gives very accurate results with the best proven L_∞-convergence; however it becomes very slow to compute for small gridsteps because its window of computations increase faster than the other estimators. **VCM** is also generic and has a proven convergence (but a quite slow theoretical convergence speed), its practical accuracy is about 3-5 times less good compared with **II**. It remains quite slow to compute without multi-threading, since it requires some volumetric computations. The elementary **C-Trivial** is also generic, much faster to compute and is almost as accurate as **II** (depending on the norm), unfortunately with no proven properties. Last, the **COV** estimator is generally as accurate in L_2-norm as **VCM**, less accurate in L_∞-norm, while being faster to compute.

Turning now to normal estimators devoted to digitized convex shapes, **CVXH** is the fastest to compute, has proven convergence (Theorem 9) but is the less accurate in practice. **I-CVXH** has proven convergence (Theorem 9 also since it is a linear convex combination of convergent estimates), and is more precise than **VCM**, competitive with **COV** and not far from **II** and **C-Trivial**, while being almost as fast as **CVXH** to compute. Finally **CI-CVXH** is almost as fast as **C-Trivial** to compute, while being at least as precise as **II** or **C-Trivial**, and is also proven convergent by the same theorem. Table 1 sums up these properties.

Computation times are given here only experimentally. However, we could theoretically establish that **CVXH** and **I-CVXH** have a smaller complexity than the other methods, since their complexity is dominated by the computation of the convex hull (hence some $\Theta(n \log n)$ for n the number of lattice points). All the other estimators have a complexity at least in $O(n(r/h))$, where the radius r/h grows to infinity as h tends to zero.

7 Geometric statistics of digitized convex hulls

Starting from 3D, you may have small or elongated facets in digitized convex hulls. This happens for instance for the two shapes studied in the previous section, `ellipsoid` and `slanted ellipsoid`. As shown on Figure 15, the average facet area is some $\Theta(h^{\frac{3}{2}})$ (since the average discrete area follows $\Theta(h^{-\frac{1}{2}})$. The average facet width (smallest side) follows $\Theta(h^{\frac{3}{4}})$ (Figure 16) while the average facet diameter (longest side) follows also $\Theta(h^{\frac{3}{4}})$ (Figure 17). It can be seen that both small facets (with bounded lattice area) and elongated facets (with bounded lattice widths) exist.

These results are in accordance with Bárány and Larman combinatorial results [40] (see also [41]) which state that, letting $P_N = \mathrm{CvxH}\left(\mathbb{Z}^d \cap NB^d\right)$ (for B^d the d-dimensional unit ball) and $f_k(P_N)$ be the number of k-dimensional faces of the lattice polytope P_N, we have $f_k(P_N) = \Theta(N^{d\frac{d-1}{d+1}})$. Let the sequence (A_i) be the area of each facet of P_N, $\bar{A}$, the average area of the facets and A, the area of the unit ball B^d. We have:

$$\begin{aligned}\bar{A} :=& \frac{1}{f_{d-1}(P_N)} \sum_{i=1}^{f_{d-1}(P_N)} A_i \\ \approx& \frac{1}{f_{d-1}(P_N)} A = \Theta\left(\frac{1}{f_{d-1}(P_N)}\right).\end{aligned}$$

In 3D, the number of facets follows $f_{d-1}(P_N) = \Theta(h^{-\frac{3}{2}})$, so the average area follows $\bar{A} = \Theta(h^{\frac{3}{2}})$, both in accordance with experiments.

Finally, as shown in Theorem 8, we can check on Figure 18 that the distance of the vertices of the digitized convex hull are very close to the smooth input shape boundary (a sphere of radius

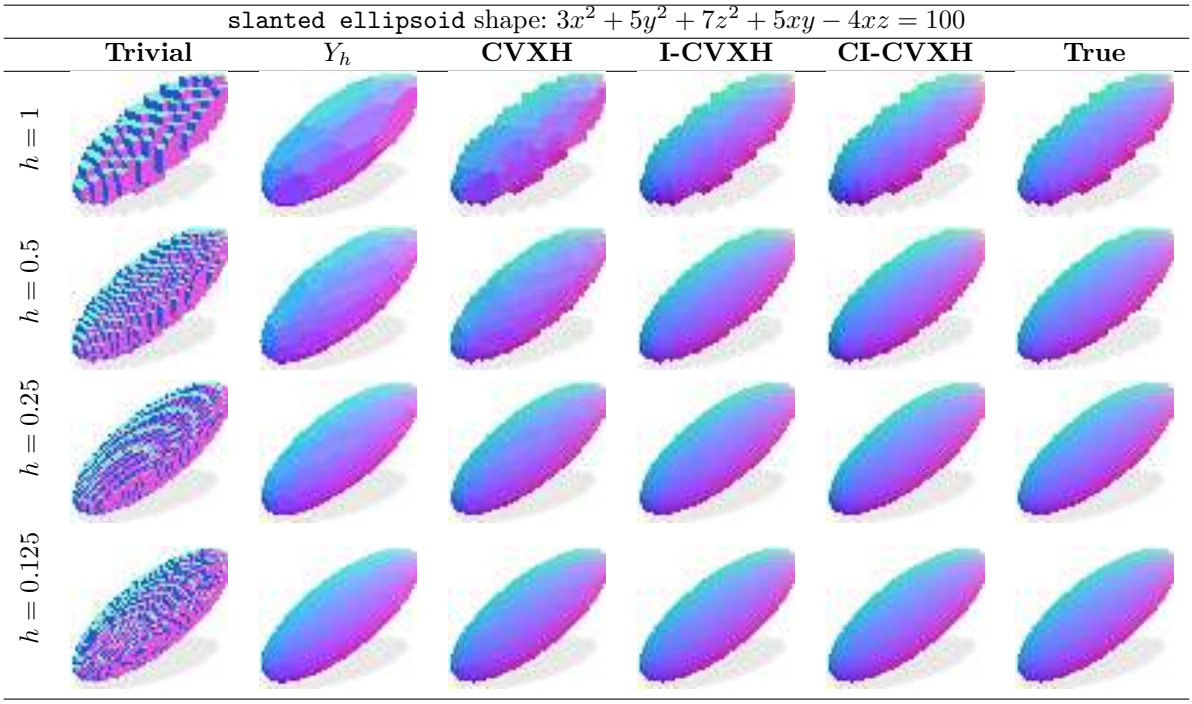

Fig. 10 Qualitative illustration of normal estimations for estimators specialized to digitized convex shapes (CVXH, I-CVXH, CI-CVXH), for finer and finer digitization of shape `slanted ellipsoid`. Normal vectors are displayed with the normal map colormap.

Table 1 Comparison between discrete normal estimators according to genericity, accuracy and computational cost (where n is the number of surfels of $\partial_h X$).

method	genericity	parameters	L_∞th./exp.	accuracy	L_2th./exp.	accuracy	comp. cost
CVXH	convex	none	$\Theta(h^{\frac{1}{2}})$	/ +	$\Theta(h^{\frac{1}{2}})$	/ +	$O(n \log n)$
I-CVXH	convex	none	$\Theta(h^{\frac{1}{2}})$	/ ++	$\Theta(h^{\frac{1}{2}})$	/ ++	$O(n \log n)$
CI-CVXH	convex	$r = \Theta(h^{\frac{1}{2}})$	$\Theta(h^{\frac{1}{2}})$	/ +++	$\Theta(h^{\frac{1}{2}})$	/ +++	$\approx O(n^{\frac{3}{2}})$
II	any	$r = \Theta(h^{\frac{1}{3}})$	$\Theta(h^{\frac{2}{3}})$	/ +++	$\Theta(h^{\frac{2}{3}})$	/ +++	$\approx O(n^{\frac{5}{3}})$
VCM	any	$R, r = \Theta(h^{\frac{1}{2}})$	$\Theta(h^{\frac{1}{8}})$	/ ++	$\Theta(h^{\frac{1}{8}})$	/ ++	$\approx O(n^{\frac{3}{2}})$
COV	any	$r = \Theta(h^{\frac{2}{3}})$	?	/ ++	$\Theta(h^{\frac{2}{3}})$	/ ++	$\approx O(n^{\frac{4}{3}})$
C-Trivial	any	$r = \Theta(h^{\frac{1}{2}})$	?	/ +++	?	/ +++	$\approx O(n^{\frac{3}{2}})$

9 and equation $x^2 + y^2 + z^2 = 9^2$). Indeed distances do not exceed $O(h^{\frac{3}{2}})$, instead of $O(h)$ for points of the digitized convex hull in general.

8 Conclusion

In this paper, we have explored links between geometrical quantities estimated on the boundary of a convex set $X \subset \mathbb{R}^d$ and similar quantities on the boundary of the convex hull of the digitization of X. We have shown the proximity of the digitized convex hull to X in terms of Hausdorff distance and highlighted that convex hull vertices are much closer to ∂X than their incident faces, explaining the visual quality of convex hulls. Our main result is that the normal vector to each facet of the digital convex hull converges towards the normal vectors of the convex shape, for small enough gridstep h, with explicit convergence speed (proportional to $\sqrt{h/\rho}$ for smooth convex shapes). This result indicates that the normal vector to facets of the digitized convex hull could be used as a discrete normal estimator on digitized convex

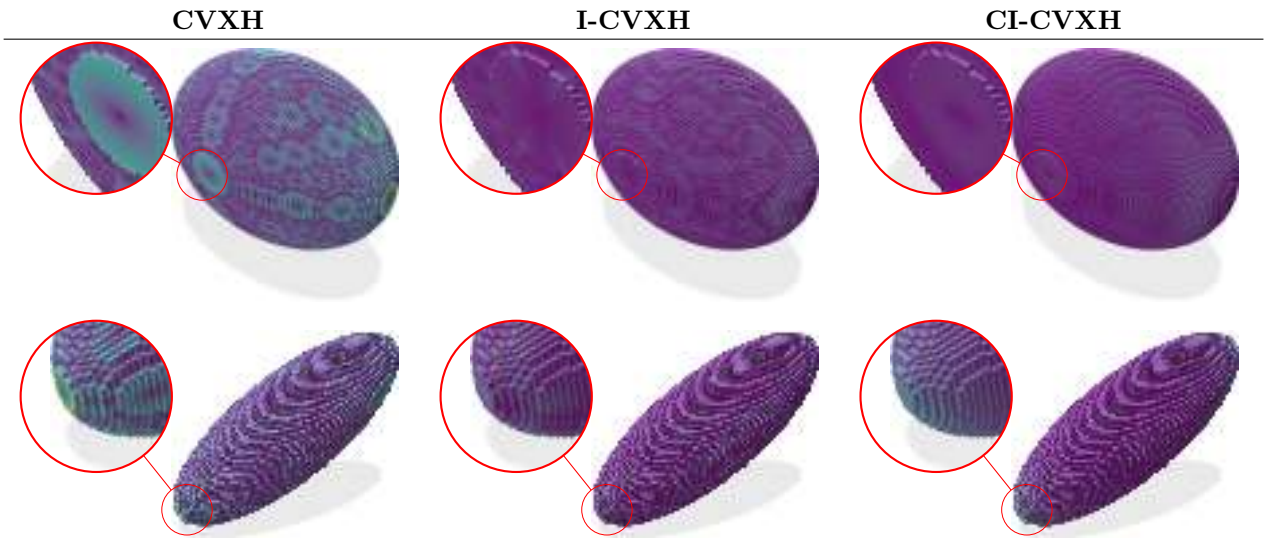

Fig. 11 For a fixed grid step ($h = 0.125$), we show normal estimation errors (in degrees) for CVXH, I-CVXH and CI-CVXH estimators on shapes `ellipsoid` (top row) and `slanted ellipsoid` (bottom row). For all methods, a fixed colormap has been used ($[0, 0.244]$ for `ellipsoid` and $[0, 0.31378]$ for `slanted ellipsoid`).

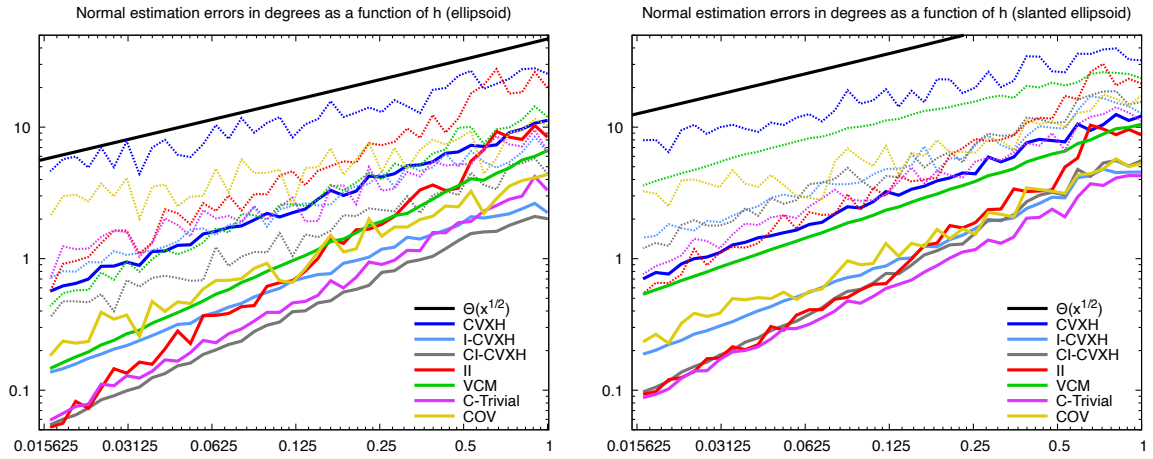

Fig. 12 Normal angle L_2-errors (L_∞-errors are drawn thinner and dashed) for different normal estimators on `ellipsoid` (left) and `slanted ellipsoid` (right) as a function of the digitization gridstep h (plots must be read from right to left as finer digitizations are to the left). See text for the definition of the normal estimators.

shapes, and more generally in convex or concave parts of digitized shapes.

This result is related to the properties of the projection function π_K onto the nearest point on a compact set K, where the difference between π_K and $\pi_{K'}$ is shown proportional to the square root of their Hausdorff distance [18, 42]. Even if we have shown that vertices are closer than $O(h)$, this is not the case elsewhere on the shape. Our achieved result is then tight, with a constant much better than the one of Voronoi Covariance Measure [18, 43], which also requires kernel integration.

Experimental evaluation of normal estimators on digitized convex shapes shows that it is much more advantageous to interpolate facet normals (I-CVXH). It then becomes a practically competitive normal estimator, fast and accurate, while staying parameter-free. Adding convolution makes it one of the most accurate estimators, yet with a

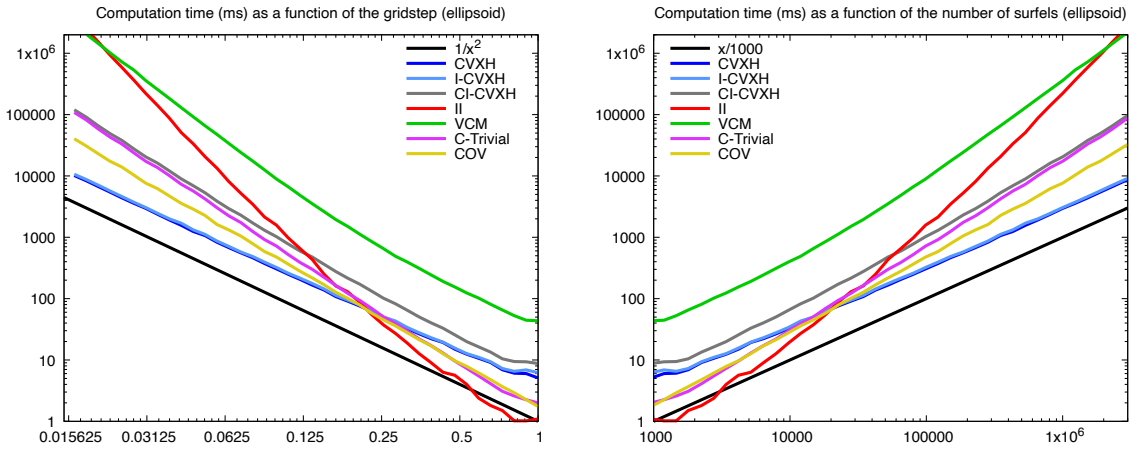

Fig. 13 Computation times (in ms) of the different normal estimators on shape `ellipsoid`: (left) as a function of the gridstep h, (right) as a function of the number of surfels n. The mirror aspect of the two diagrams is expected since $n = \Theta(h^{-2})$ on a digitized boundary surface.

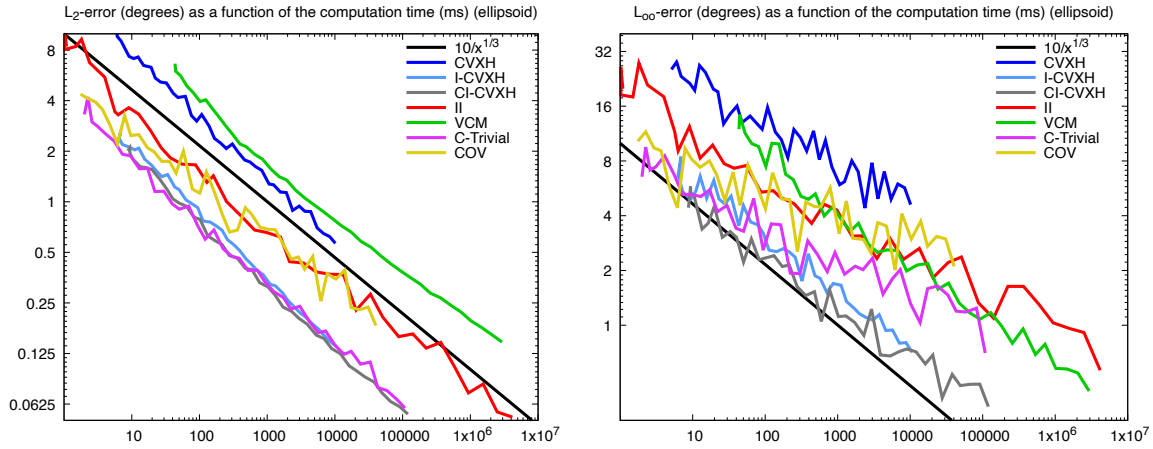

Fig. 14 Normal angle estimation error (in degrees) as a function of the computation time (in ms): (left) L_2-error, (right) L_∞-error. A good estimator can achieve low error with as little computation effort as possible, hence its plot should be decreasing as fast as possible in the bottom left corner.

slightly slower convergence speed than II estimator for very fine gridsteps. Finally the C-Trivial estimator appears as a surprisingly simple and accurate estimator, and proving its multigrid convergence is one line of work we wish to pursue in the future.

Acknowledgements. This work is partially supported by the French National Research Agency within the StableProxies project (ANR-22-CE46-0006).

References

[1] Stelldinger, P., Köthe, U.: Towards a general sampling theory for shape preservation. Image and Vision Computing **23**(2), 237–248 (2005)

[2] Stelldinger, P., Latecki, L.J., Siqueira, M.: Topological equivalence between a 3d object and the reconstruction of its digital image. IEEE transactions on pattern analysis and machine intelligence **29**(1), 126–140 (2006)

[3] Huxley, M.N.: Area, Lattice Points, and

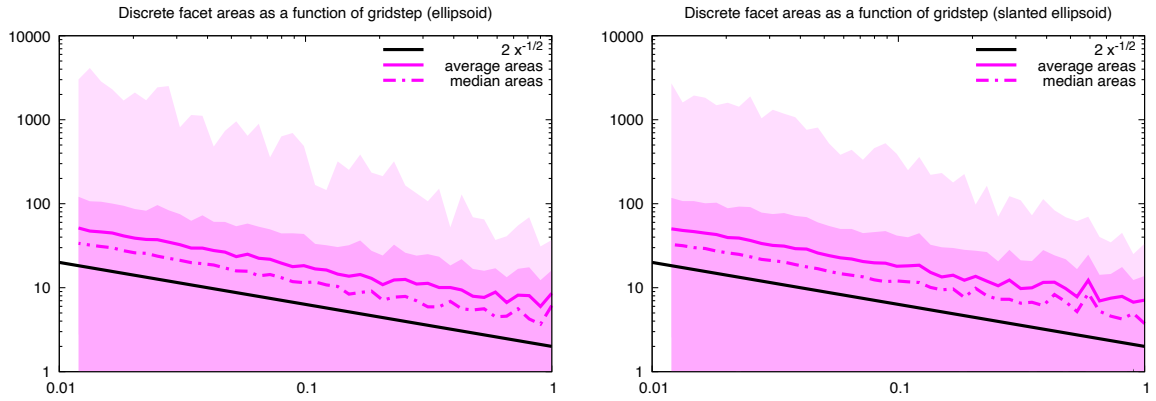

Fig. 15 Facet areas of the digitized convex hull of `ellipsoid` (left) and `slanted ellipsoid` (right), as a function of h: average and median areas are displayed, the darker band corresponds to facet areas within the standard deviation of the average edge lengths, while the lighter band corresponds to minimum and maximum.

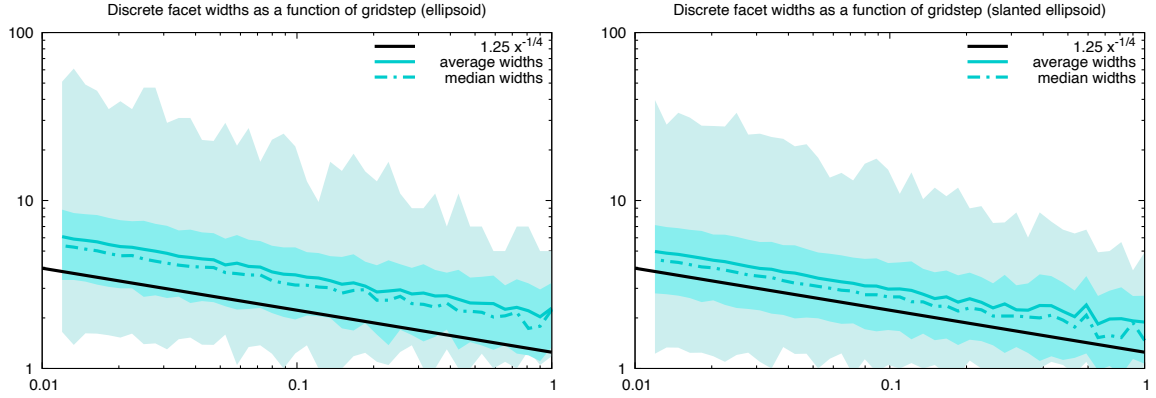

Fig. 16 Facet widths of the digitized convex hull of `ellipsoid` (left) and `slanted ellipsoid` (right), as a function of h: average and median widths are displayed, the darker band corresponds to facet widths within the standard deviation of the average edge lengths, while the lighter band corresponds to minimum and maximum.

Exponential Sums. London Mathematical Soceity Monographs New Series, Oxford Science Publications, vol. 13. UK (1996)

[4] Klette, R., Žunić, J.: Multigrid convergence of calculated features in image analysis. Journal of Mathematical Imaging and Vision **13**, 173–191 (2000)

[5] Lachaud, J.-O., Thibert, B.: Properties of gauss digitized shapes and digital surface integration. Journal of Mathematical Imaging and Vision **54**(2), 162–180 (2016) https://doi.org/10.1007/s10851-015-0595-7

[6] Klette, R., Rosenfeld, A.: Digital straightness — a review. Discrete applied mathematics **139**(1-3), 197–230 (2004)

[7] Brimkov, V., Coeurjolly, D., Klette, R.: Digital planarity—a review. Discrete Applied Mathematics **155**(4), 468–495 (2007)

[8] Kim, C.E.: Digital convexity, straightness, and convex polygons. IEEE Transactions on Pattern Analysis and Machine Intelligence (6), 618–626 (1982)

[9] Fernique, T.: Generation and recognition of digital planes using multi-dimensional continued fractions. Pattern Recognition **42**(10), 2229–2238 (2009)

[10] Lachaud, J.-O., Provençal, X., Roussillon, T.:

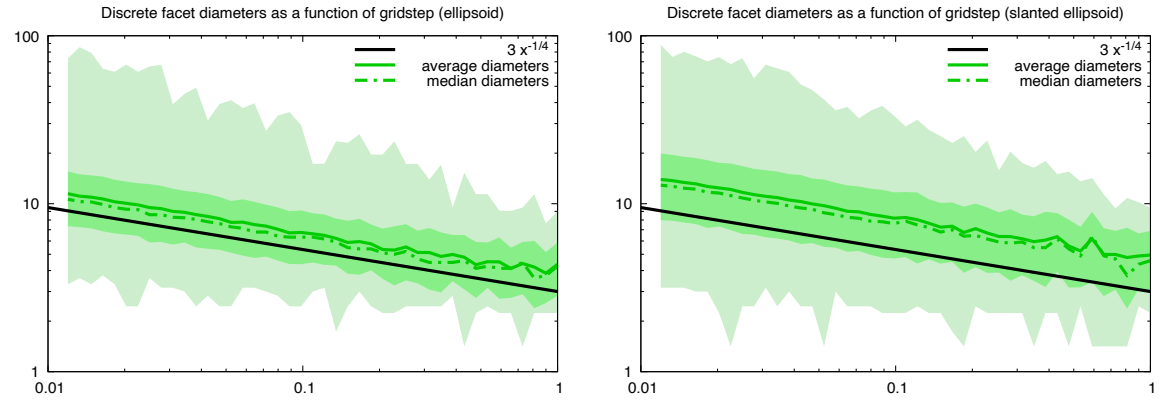

Fig. 17 Facet diameters of the digitized convex hull of `ellipsoid` (left) and `slanted ellipsoid` (right), as a function of h: average and median diameters are displayed, the darker band corresponds to facet diameters within the standard deviation of the average edge lengths, while the lighter band corresponds to minimum and maximum.

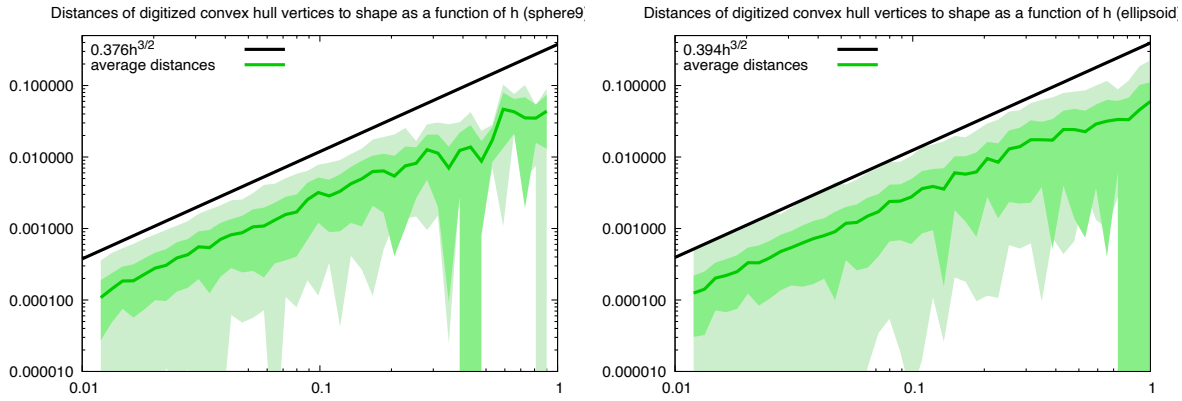

Fig. 18 Distance of digitized convex hull vertices to input `sphere9` shape (left) and `ellipsoid` shape (right), as a function of the gridstep h: convex hull vertices are much closer to the smooth input shape boundary than most digitized points, i.e. $O(h^{\frac{3}{2}})$. The expected constant is $2/\sqrt{\pi\rho}$, that is $2/\sqrt{9\pi} \approx 0.376$ for `sphere9` and $2/\sqrt{45\pi/\sqrt{30}} \approx 0.394$ for `ellipsoid`. Lightest green zone indicates min/max values, medium green zone indicates the standard deviation around the median value.

Two plane-probing algorithms for the computation of the normal vector to a digital plane. Journal of Mathematical Imaging and Vision **59**(1), 23–39 (2017)

[11] Lu, J.-T., Roussillon, T., Lachaud, J.-O., Coeurjolly, D.: Delaunay property and proximity results of the L-algorithm for digital plane probing. Theoretical Computer Science **1011**, 114719 (2024)

[12] Esbelin, H.-A., Malgouyres, R.: Convergence of binomial-based derivative estimation for C2 noisy discretized curves. In: Discrete Geometry for Computer Imagery: 15th IAPR International Conference, DGCI 2009, Montréal, Canada, September 30-October 2, 2009., pp. 57–66 (2009). Springer

[13] Provot, L., Gérard, Y.: Estimation of the derivatives of a digital function with a convergent bounded error. In: International Conference on Discrete Geometry for Computer Imagery, pp. 284–295 (2011). Springer

[14] Lachaud, J.-O., Vialard, A., Vieilleville, F.: Fast, accurate and convergent tangent estimation on digital contours. Image and Vision Computing **25**(10), 1572–1587 (2007)

[15] Fourey, S., Malgouyres, R.: Normals estimation for digital surfaces based on convolutions. Computers & Graphics **33**(1), 2–10 (2009)

[16] Tellier, P., Debled-Rennesson, I.: 3d discrete normal vectors. In: Discrete Geometry for Computer Imagery: 8th International Conference, DGCI'99 Marne-la-Vallée, France, March 17–19, 1999, pp. 447–458 (1999). Springer

[17] Lachaud, J.-O., Vialard, A.: Geometric measures on arbitrary dimensional digital surfaces. In: Discrete Geometry for Computer Imagery: 11th International Conference, DGCI 2003, Naples, Italy, November 19-21, 2003, pp. 434–443 (2003). Springer

[18] Mérigot, Q., Ovsjanikov, M., Guibas, L.J.: Voronoi-based curvature and feature estimation from point clouds. IEEE Transactions on Visualization and Computer Graphics **17**(6), 743–756 (2010)

[19] Cuel, L., Lachaud, J.-O., Thibert, B.: Voronoi-based geometry estimator for 3d digital surfaces. In: Barcucci, E., Frosini, A., Rinaldi, S. (eds.) Proc. Int. Conf. on Discrete Geometry for Computer Imagery (DGCI'2014), Sienna, Italy. Lecture Notes in Computer Science, vol. 8668, pp. 134–149. Springer, Cham (2014). https://doi.org/10.1007/978-3-319-09955-2_12

[20] Pottmann, H., Wallner, J., Yang, Y.-L., Lai, Y.-K., Hu, S.-M.: Principal curvatures from the integral invariant viewpoint. Computer Aided Geometric Design **24**(8-9), 428–442 (2007)

[21] Lachaud, J.-O., Coeurjolly, D., Levallois, J.: Robust and convergent curvature and normal estimators with digital integral invariants. In: Najman, L., Romon, P. (eds.) Modern Approaches to Discrete Curvature. Lecture Notes in Mathematics, vol. 2184, pp. 293–348. Springer, Cham (2017). https://doi.org/10.1007/978-3-319-58002-9_9

[22] Coeurjolly, D., Klette, R.: A comparative evaluation of length estimators of digital curves. IEEE transactions on pattern analysis and machine intelligence **26**(2), 252–258 (2004)

[23] De Vieilleville, F., Lachaud, J.-O., Feschet, F.: Convex digital polygons, maximal digital straight segments and convergence of discrete geometric estimators. Journal of Mathematical Imaging and Vision **27**, 139–156 (2007)

[24] De Loera, J.A.: The many aspects of counting lattice points in polytopes. Mathematische Semesterberichte **52**(2), 175–195 (2005)

[25] Beck, M., Robins, S.: Computing the Continuous Discretely: Integer-point Enumeration in Polyhedra vol. 2. Springer, Cham (2007)

[26] Böröczky Jr, K.: Approximation of general smooth convex bodies. Advances in Mathematics **153**(2), 325–341 (2000)

[27] Lachaud, J., Coeurjolly, D., Roussillon, T.: Geometry of gauss digitized convex shapes. In: Wilkinson, M.H.F., Kosinka, J. (eds.) Discrete Geometry and Mathematical Morphology - 4th International Joint Conference, DGMM 2025, Groningen, The Netherlands, November 3-6, 2025, Proceedings. Lecture Notes in Computer Science, vol. 16296, pp. 16–30. Springer, Cham (2025). https://doi.org/10.1007/978-3-032-09544-2_2

[28] Schneider, R.: Convex Bodies: the Brunn–Minkowski Theory vol. 151. Cambridge university press, Cambridge, UK (2013)

[29] Reeve, J.E.: On the volume of lattice polyhedra. Proceedings of the London Mathematical Society **3**(1), 378–395 (1957)

[30] Balog, A., Bárány, I.: On the convex hull of the integer points in a disc. In: Proceedings of the 7th Annual Symposium on Computational Geometry, pp. 162–165 (1991)

[31] Federer, H.: Curvature measures. Transactions of the American Mathematical Society **93**(3), 418–491 (1959)

[32] Wills, M.D.: Hausdorff distance and convex

sets. Journal of Convex Analysis **14**(1), 109–117 (2007)

[33] Macbeath, A.M.: A theorem on non-homogeneous lattices. Annals of Mathematics **56**(2), 269–293 (1952)

[34] Bárány, I.: Random points, convex bodies, lattices. arXiv preprint math/0304462 (2003). ICM 2002

[35] Minkowski, H.: Geometrie der Zahlen. Teubner, Leipzig (1896). §30

[36] Coeurjolly, D., Lachaud, J.-O., Levallois, J.: Multigrid convergent principal curvature estimators in digital geometry. Computer Vision and Image Understanding **129**, 27–41 (2014) https://doi.org/10.1016/j.cviu.2014.04.013

[37] Mitra, N.J., Nguyen, A.: Estimating surface normals in noisy point cloud data. In: Proceedings of the Nineteenth Annual Symposium on Computational Geometry (SoCG'03), San Diego, California, pp. 322–328 (2003)

[38] Papier, L., Françon, J.: Evaluation de la normale au bord d'un objet discret 3d. Revue internationale de CFAO et d'informatique graphique **13**(2), 205–226 (1998)

[39] DGtal: Digital Geometry tools and algorithms library. https://dgtal.org, release 2.1

[40] Bárány, I., Larman, D.G.: The convex hull of the integer points in a large ball. Mathematische Annalen **312**, 167–181 (1998)

[41] Bárány, I.: Random points and lattice points in convex bodies. Bulletin of the American Mathematical Society **45**(3), 339–365 (2008)

[42] Chazal, F., Cohen-Steiner, D., Mérigot, Q.: Boundary measures for geometric inference. Foundations of Computational Mathematics **10**, 221–240 (2010)

[43] Mérigot, Q., Ovsjanikov, M., Guibas, L.: Robust voronoi-based curvature and feature estimation. In: 2009 SIAM/ACM Joint Conference on Geometric and Physical Modeling, pp. 1–12 (2009)

A Proofs of some properties

Recall of Corollary 3. *Let $(\mathbf{z}, \mathbf{z}')$ be a surfel of X_h. Let $\mathbf{y}$ be the nearest point on ∂Y_h to $\mathbf{z}'$ and let σ be a facet of Y_h containing $\mathbf{y}$, with normal vector $\mathbf{n}_\sigma$. We have:*

- *there exists $\mathbf{x} \in \partial X \cap [\mathbf{y}, \mathbf{z}'[$, that is at distance less than h from $\mathbf{y}$,*
- *for any $\mathbf{n} \in \mathrm{N}_X(\mathbf{x})$, $\sin^2 \angle(\mathbf{n}, \mathbf{n}_\sigma) \leqslant \frac{1}{1+(r/h)^2}$, if $r := \mathrm{d}_{\mathbf{E}}(\mathbf{y}, \partial\sigma)$.*

Proof We have $\|\mathbf{y} - \mathbf{z}'\| \leqslant \|\mathbf{z} - \mathbf{z}'\| = h$ since $\mathbf{y}$ is the closest point of Y_h to $\mathbf{z}'$ and $\mathbf{z}$ belongs also to Y_h. Since $\mathbf{y} \in Y_h = \mathrm{CvxH}(X_h) \subset \mathrm{CvxH}(X) = X$ and $\mathbf{z}' \notin X_h$ so $\mathbf{z}' \notin X$, there must be a point $\mathbf{x}$ on the boundary of X on the straight segment joining $\mathbf{y}$ to $\mathbf{z}'$. It follows that $\|\mathbf{y} - \mathbf{x}\| < \|\mathbf{y} - \mathbf{z}'\| \leqslant h$, the strict relation coming from $\mathbf{x} \neq \mathbf{z}'$. The relation between normal vectors follows from Lemma 2, replacing ϵ with the distance h, if $\mathbf{y}$ lies in the interior of the facet σ. However if $\mathbf{y} \in \partial\sigma$, then $r := \mathrm{d}_{\mathbf{E}}(\mathbf{y}, \partial\sigma) = 0$, and the angle relation reduces to $\sin^2 \angle(\mathbf{n}, \mathbf{n}_\sigma) \leqslant 1$, which is always true. □

Recall of Corollary 7. *For all gridsteps h, $0 < h < \frac{2\rho}{\sqrt{d}}$, for $\mathbf{y} \in \partial Y_h$ and any normal vector $\mathbf{w} \in \mathrm{N}_{Y_h}(\mathbf{y})$, define P as the plane orthogonal to $\mathbf{w}$ and containing $\mathbf{y}$. then for any point $\mathbf{y}' \in P$, we have that $\mathbf{y}' + t\mathbf{w}$ is outside X for $t > \sqrt{d}h$.*

Proof Indeed $\mathbf{w} \in \mathrm{N}_{Y_h}(\mathbf{y})$ implies by definition that $\phi_{Y_h}(\mathbf{w}) = \mathbf{y} \cdot \mathbf{w}$. The Hausdorff distance between Y_h and X is less than $\sqrt{d}h$ (Theorem 6), so

$$\phi_X(\mathbf{w}) \leq \phi_{Y_h}(\mathbf{w}) + \sqrt{d}h. \tag{8}$$

Let $\mathbf{y}'' := \mathbf{y}' + t\mathbf{w}$, for $t > \sqrt{d}h$. Observe that $\mathbf{y}' \cdot \mathbf{w} = \mathbf{y} \cdot \mathbf{w}$ since $\mathbf{y}'$ belongs to P. It follows that $\mathbf{y}'' \cdot \mathbf{w} = \mathbf{y}' \cdot \mathbf{w} + t\mathbf{w} \cdot \mathbf{w} = \mathbf{y} \cdot \mathbf{w} + t \geqslant \phi_{Y_h}(\mathbf{w}) + \sqrt{d}h$. Using (8), we get $\mathbf{y}'' \cdot \mathbf{w} > \phi_X(\mathbf{w})$ and $\mathbf{y}' \notin X$ by definition of the support function. □